Geol. Mag. **143** (*1*), *2006, pp. 59–88.* © *2006 Cambridge University Press*
doi:10.1017/S0016756805001433 *Printed in the United Kingdom*

Structural evolution and tectonic setting of the Porongos belt, southern Brazil

K. SAALMANN*, M. V. D. REMUS† & L. A. HARTMANN†

*Geologisch-Paläontologisches Institut, J. W. Goethe-Univ. Frankfurt, Senckenberganlage 32–34, D-60054 Frankfurt am Main, Germany
†Instituto de Geociéncias, Universidade Federal do Rio Grande do Sul, Caixa Postal 15001 CEP 91501-970, Porto Alègre, RS, Brazil

(*Received* 16 August 2004; *revised version received* 13 June 2005; *accepted* 28 June 2005)

Abstract – The SW–NE-striking Porongos belt, located between juvenile Neoproterozoic rocks in the west and the Dom Feliciano belt, characterized by intense reworking of older crust, in the east, comprises a greenschist to amphibolite-facies metavolcano-metasedimentary succession (Porongos sequence) of unknown age with some exposures of Palaeoproterozoic gneisses (Encantadas gneisses). High-temperature ductile deformation of the basement gneisses comprises at least two magmatic events followed by three deformational phases including folding and shearing (D_T1–D_T3) and can be attributed to the Palaeoproterozoic Trans-Amazonian orogeny. The deformation of the Porongos sequence occurred during the Neoproterozoic Brasiliano orogeny and comprises four ductile deformation phases (D_B1–D_B4), including two phases of isoclinal folding associated with shearing recorded in mylonitic layers, followed by closed NW-vergent folding and thrusting leading to formation of a thrust stack. Uplift of the basement and formation of late tectonic sedimentary basins occurred as a result of semi-ductile to brittle block faulting in a sinistral strike-slip regime. The Porongos sequence can be subdivided into a southeastern and a northwestern part. Trace element analyses as well as Sm–Nd and Rb–Sr geochemical data indicate partial melting and significant contamination by old continental crust for the metavolcanic rocks. The metavolcanic rocks show $\varepsilon Nd(t = 780\ Ma)$ values of -20.64 and -21.72 (northwestern units) and -6.87 (southeastern sequence). The metasedimentary rocks were derived from late Palaeoproterozoic to Archaean sources, and the data indicate different sources for the northwestern and southeastern rock units of the Porongos sequence. $\varepsilon Nd(t = 780\ Ma)$ are -6.25 and -6.85 in the southeastern units, with TDM model ages between 1734 and 1954 Ma, and vary between -14.72 and -17.96 in the northwestern parts, which have TDM model ages between 2346 and 2710 Ma. High $^{87}Sr/^{86}Sr(t)$ values between 0.7064 and 0.7286 confirm reworking of older crust. Isotopic signatures of the Porongos sequence do not show indications for a significant contribution from a Neoproterozoic juvenile source. A passive margin or continental rift environment is suggested for the tectonic setting of the Porongos belt, which is compatible with both deposition of shallow marine to deep marine sediments and stretching of continental crust leading to volcanism which is characterized by significant contamination by old continental crust.

Keywords: West Gondwana, Neoproterozoic, Brasiliano orogeny, Nd model age, tectonics.

1. Introduction

The reconstruction of the amalgamation of West Gondwana (Fig. 1a), a mosaic made of Archaean and Palaeo- and Mesoproterozoic cratonic nucleii, still holds uncertainties in the timing and structural mechanisms of collisional events between different crustal blocks and cratons. Unknown occurrence and width of former oceanic basins and insufficient precise ages of orogenic belts greatly limit the understanding of the assembly. Moreover, any tectonic model without or only insufficient consideration of structural data remains disputable.

* Author for correspondence: Kerstin.Saalmann@gtk.fi; present address: Geological Survey of Finland, PO Box 96, FIN-02151 Espoo, Finland

Despite a great number of studies during the last decades, little attention was paid to the South American Rio de la Plata craton, and compared to other areas, only limited geological and geochronological data from the Rio de la Plata craton and its surroundings are published, leading to diverging palaeogeographic reconstructions. However, the study of the tectonic evolution of the Rio de la Plata craton and its surrounding Neoproterozoic mobile belts is essential to unravelling its role and position relative to other South American and African cratons in the period between the Rodinia assembly and break-up and the amalgamation of Gondwana.

Studies on the tectonic evolution of southern Brazil focus mainly on the age and geochemistry of plutonic rocks and gneisses. Published studies with detailed

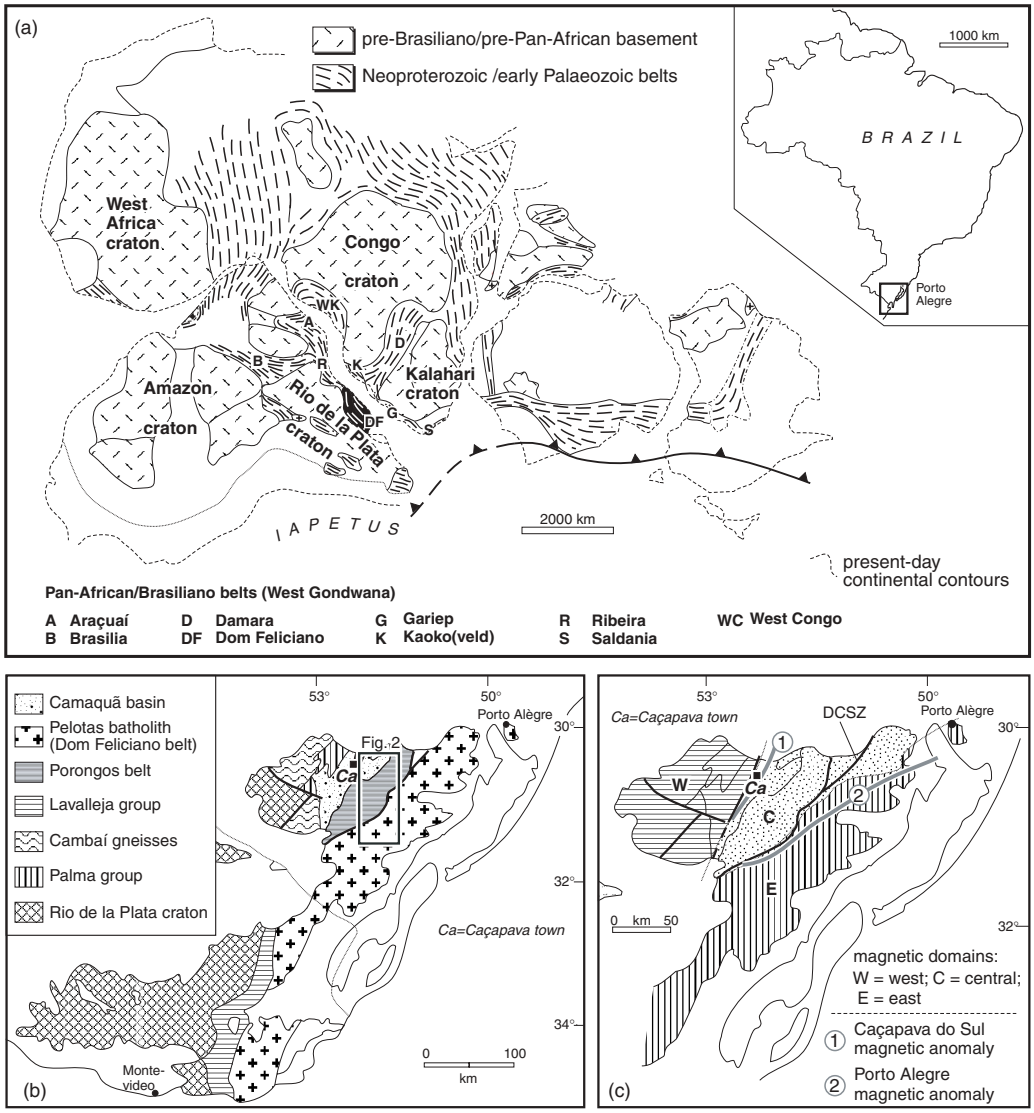

Figure 1. (a) 500 Ma reconstruction of Gondwana with Neoproterozoic mobile belts (modified from Trompette, 1994 and Unrug, 1997); note the position of Rio Grande do Sul Neoproterozoic mobile belts (black). (b) Geological map with the tectonic domains of southern Brazil (modified from Fernandes, Tommasi & Porcher, 1992 and Chemale, Hartmann & da Silva, 1995). (c) Geophysical domains based on magnetic and gravimetric data (simplified after A.F.U. Costa, unpub. Ph.D. thesis, Univ. Rio Grande do Sul, 1997 and Chemale, 2000) (DCSZ = Dorsal de Canguçu Shear Zone).

structural data are rare, and thus no consistent plate tectonic model for this area exists up to now. In particular, the schist belts have been much less studied so that their structure, age and tectonic setting are still unclear. Schist belts, however, contain a large volume of information about the structural evolution and the kinematics of deformations which are essential for the study of the collisional history. Plate tectonic models for southern Brazil differ markedly. Despite many U–Pb studies on igneous rocks and orthogneisses in southern Brazil, isotopic studies of different belts including their basement complexes still need refinement. The identification of terranes, their structural evolution and the timing of collisional events are important for establishing a plate tectonic model and thus for studies concerning a regional and global view of Gondwana amalgamation.

Precambrian rocks of Brazil's southernmost state, Rio Grande do Sul, have had a complex tectono-metamorphic evolution since the Archaean (Silva *et al.* 2000; Hartmann *et al.* 1999, 2000; Chemale, 2000). Major crustal accretion and cratonization occurred during the 2.2–2.0 Ga Trans-Amazonian orogeny which represents an important orogenic event in southern Brazil (Hartmann *et al.* 2000; Santos *et al.* 2003). Neoproterozoic events related to the amalgamation of West Gondwana belong to the Brasiliano/Pan-African orogenic cycle.

Based on lithostratigraphy, petrography, geophysical data and geochemistry, a number of major

tectono-stratigraphic units can be distinguished (Jost & Hartmann, 1984; Chemale, Hartmann & da Silva, 1995; Hartmann *et al.* 1999) (Fig. 1b).

The granite-gneiss unit in the east (Dom Feliciano belt) is characterized by extensive Neoproterozoic crustal reworking of Trans-Amazonian (2.2–2.0 Ga) gneisses (Babinski *et al.* 1996, 1997; Silva *et al.* 1999, 2000; Hartmann *et al.* 2000). It contains numerous and voluminous *c.* 630–600 Ma Neoproterozoic granitoids. To the west, this unit is bordered by a broad ductile sinistral transcurrent shear zone, the Dorsal de Canguçu Shear Zone (DCSZ) (Tommasi *et al.* 1994; Koester *et al.* 1997; Fernandes & Koester, 1999), which is intruded by a number of synkinematic granites. Greenschist- to amphibolite-facies supracrustal rocks of unknown age with some exposures of Palaeoproterozoic gneisses are exposed to the west of the shear zone. They are part of the Porongos belt. The western border of this belt is covered by unmetamorphosed sedimentary and volcanic rocks of late Neoproterozoic to early Palaeozoic age (Camaqã molasse basin). Juvenile Neoproterozoic calc-alkaline orthogneisses and metamorphosed volcano-sedimentary rocks are exposed in the western part of the Southern Brazilian Shield (Babinski *et al.* 1996; Leite *et al.* 1998; Saalmann *et al.* 2005). They form the São Gabriel Block. This block is bounded to the east and south by Archaean to Palaeoproterozoic gneisses and granulites (Taquarembó block) which are part of the Rio de la Plata craton (Hartmann, 1998; Hartmann *et al.* 1999).

Three major tectono-magmatic events can be distinguished (Babinski *et al.* 1996, 1997; Leite *et al.* 1998; Hartmann *et al.* 1999, 2000): the *c.* 880 Ma Passinho event and the 750–700 Ma São Gabriel event, both representing accretion of magmatic arcs, and the ~ 630–600 Ma Dom Feliciano event.

Despite extensive geological mapping and many isotopic and geochemical studies, a consistent plate tectonic model for the Neoproterozoic Brasiliano orogeny in this area is still lacking. High-precision Pb–Pb and U–Pb zircon ages, comprising both conventional and sensitive, high-resolution ion-microprobe (SHRIMP) data, are now available from a number of granitoid rocks in Rio Grande do Sul (e.g. Babinski *et al.* 1996, 1997; Leite *et al.* 1998, 2000; Silva *et al.* 1999; Hartmann *et al.* 1999, 2000; Remus *et al.* 2000*a*). They focus on plutonic rocks in the São Gabriel block and Dom Feliciano belt, whereas only limited reliable isotope data are available for the Porongos belt. Despite extensive geochronological studies in Rio Grande do Sul in the last ten years, little is known about the tectonic setting and structural evolution of the Porongos belt.

This study focuses on the Santana da Boa Vista region, located in the central portion of the Porongos belt, and provides data on the structural geology combined with geochemical and isotopic data (Sm–Nd, Rb–Sr). The latter are of a preliminary nature because the number of samples is too small to be representative. Nevertheless, they present first results and may serve as impetus for further detailed studies. The aim is to present the structural geometry and evolution of this area in order to present a plate tectonic model for the Pan-African/Brasiliano orogenic cycle in this region. The data have implications for comparison with other tectono-stratigraphic units of the Southern Brazilian Shield as well as for correlation with Brasiliano belts in Uruguay and Brazil, crucial for unravelling the plate tectonic puzzle of the amalgamation of Gondwana.

2. Geological overview and stratigraphy

2.a. Geology of the Porongos belt

The Porongos belt is a SW–NE-oriented schist belt (Fig. 2). It is bounded to the east by the Dom Feliciano belt, with the tectonic contact being represented by the transcurrent DCSZ. To the west, normal and strike-slip faults separate the belt from late Neoproterozoic to Cambrian volcanic and sedimentary rocks of the Camaquã basin. The northern and southern continuations are covered by post-Brasiliano Phanerozoic sedimentary rocks.

The age of the Porongos belt is ambiguous. It has been interpreted as part of the Tijucas belt (Hasui *et al.* 1975) and thus would be equivalent to the Brusque Complex situated 700 km to the northeast in Santa Catarina (Jost & Bitencourt, 1980; Almeida, Brito Neves & Carneiro, 2000). It has also been correlated with the Las Tetas Complex located some 400 km to the south in Uruguay (Hartmann *et al.* 2001). Both correlations would imply that the Porongos belt could be older than late Neoproterozoic.

The Porongos belt can be divided into a western and an eastern part separated by narrow fault-bounded graben filled with siliciclastic Camaquã sediments of the Piquiri and Guaritas basins (Fig. 2) as well as by outcrops of pre-Brasiliano gneissic rocks which are preferentially exposed in the central areas, namely in the cores of regional SW–NE-trending antiforms (Jost & Bitencourt, 1980) (e.g. Capané and Santana antiforms) (Fig. 2).

The Porongos belt is made up of several geological units (Figs 2, 3):

(1) The pre-Brasiliano basement is represented by the Encantadas Complex (Porcher & Fernandes, 1990; Remus *et al.* 1990; Tommasi *et al.* 1994), which is mainly exposed in the core of the Porongos belt. It comprises: (a) dioritic, tonalitic and granodioritic gneisses (Encantadas gneisses); (b) mylonitized syenogranites and monzogranites; (c) lens-shaped amphibolites on a tens to hundreds of metres scale within the Encantadas gneisses.

The Encantadas Complex is a tonalite–trondhjemite–granodiorite association formed during the Palaeoproterozoic Trans-Amazonian orogeny (Hartmann

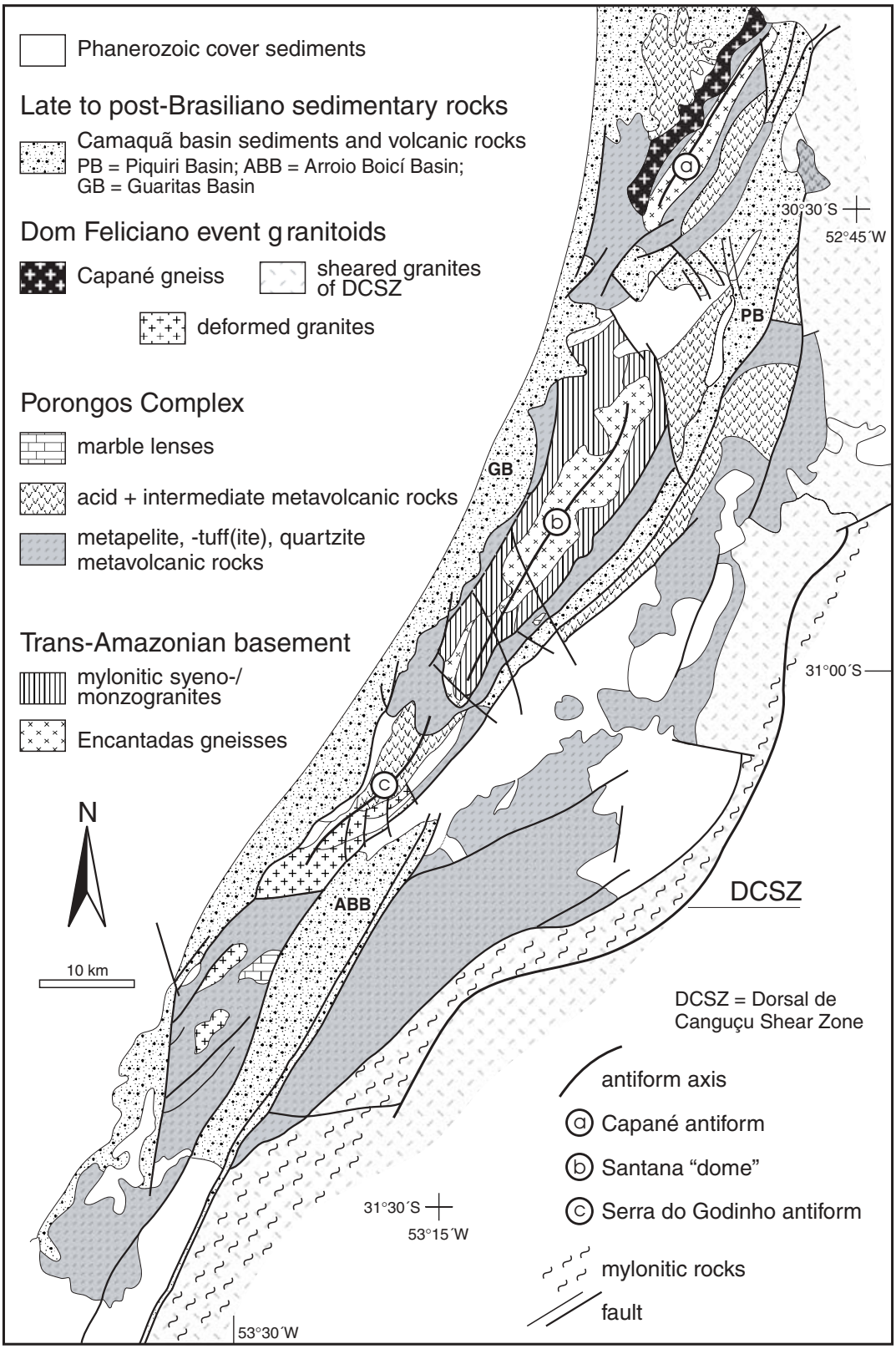

Figure 2. Geological map of the Porongos belt (modified after Chemale, 2000). The study area is located in the Santana antiform (b).

et al. 1999). Zircon U–Pb analyses (SHRIMP) of the Encantadas gneisses (Santana da Boa Vista area), of a tonalitic gneiss and a pegmatite, indicate magmatic crystallization ages of 2263 ± 18 Ma and 2363 ± 6 Ma, respectively (Porcher *et al. in* Hartmann, Porcher & Remus, 2000). Ages of 2045 ± 10 Ma and 2021 ± 11 Ma obtained from metamorphic zircon grains in these rocks represent the age of metamorphism (Hartmann,

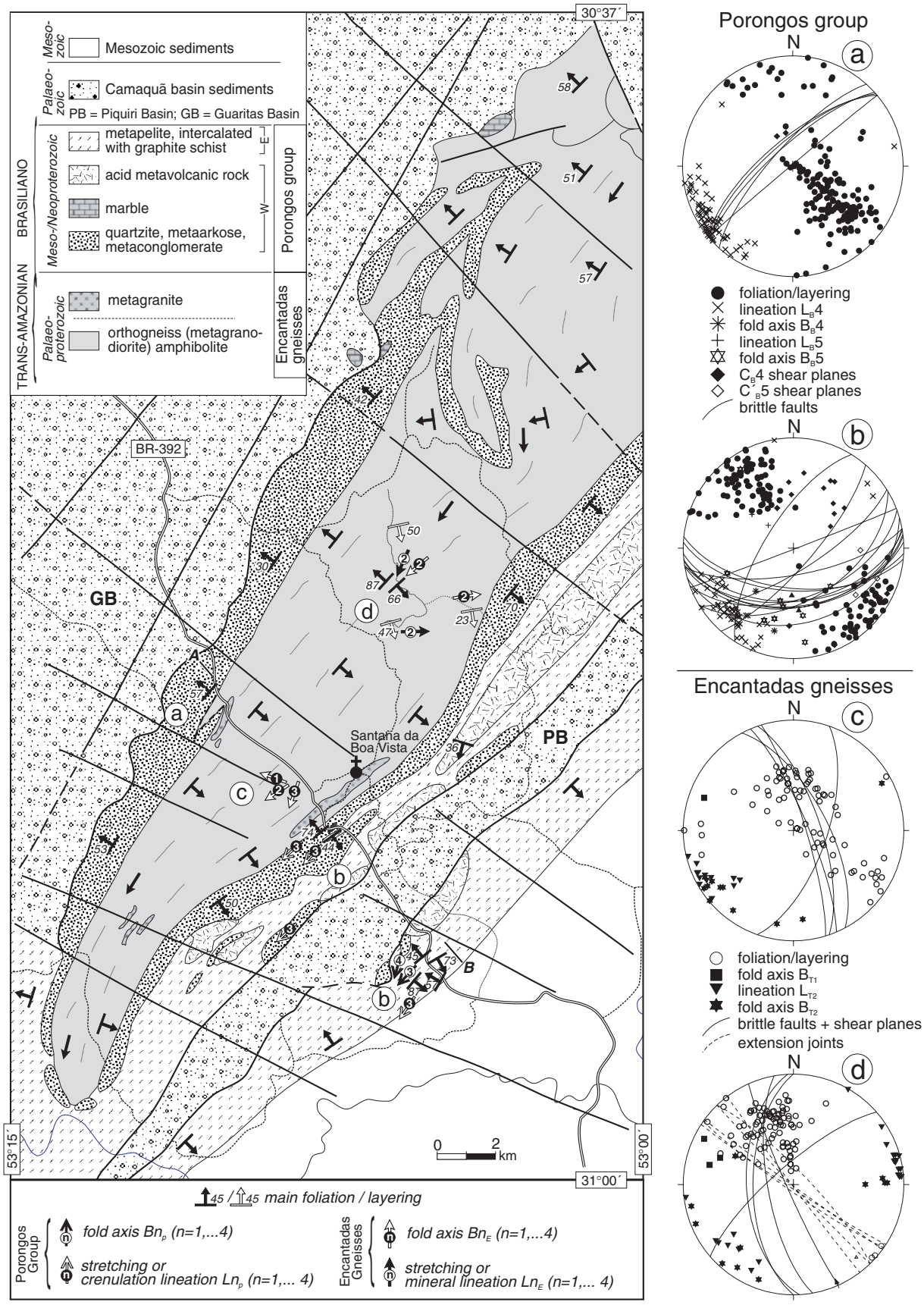

Figure 3. Geological map of the Santana da Boa Vista area and Santana antiform (modified after Remus *et al.* 1990). (a) to (d) mark the area for structural data presented in lower hemisphere stereoplots to the right. For NW–SE section *A–B* (subparallel to road BR-392), see Figure 4.

Porcher & Remus, 2000). The Encantadas gneisses are proposed to represent relics of Palaeoproterozoic island arcs that consolidated onto an older continent (Hartmann *et al.* 1999).

(2) The supracrustal Porongos group consists of greenschist- to amphibolite-facies metavolcanic and metasedimentary rocks of Meso- or Neoproterozoic age. It comprises metapelites, quartzites and felsic to intermediate metavolcanic rocks (Jost & Bitencourt, 1980; Remus *et al.* 1987; Porcher & Fernandes, 1990; Remus, Hartmann & Ribeiro, 1991) associated with mylonitized granites (Porcher & Fernandes, 1990). The latter are interpreted as pre- to syntectonic to the dominant deformation of the Porongos belt (Remus *et al.* 1987; Remus, Hartmann & Ribeiro, 1991; Porcher & Fernandes, 1990). Subordinate intercalations are marble, graphite schist, meta-arkose and metaconglomerate, as well as lenses of ultramafic rocks (serpentinite, talc schist, chlorite schist) (Jost & Bitencourt, 1980; Remus, Hartmann & Ribeiro, 1991).

(3) Deformed syntectonic granites, such as the Capané gneiss, have ages of 543 ± 6 Ma (conventional U–Pb zircon) (Chemale, 2000).

(4) The schists and gneisses are truncated by steeply inclined semi-ductile to brittle transcurrent faults. The fault-bounded Piquiri and Guaritas basins are filled with unmetamorphosed siliciclastic sediments which were deformed by faulting and folding (Paim, Chemale & Lopes, 2000).

The Trans-Amazonian basement (Encantadas Complex) is exposed in the cores of antiforms in the central parts of the Porongos belt (Fig. 2). The western and eastern contacts of the high-grade metamorphic basement to the greenschist- to lower amphibolite-grade metavolcano-sedimentary Porongos sequence are represented by semi-brittle to brittle faults (Figs 3, 4). With decreasing distance to the contact, the number of brittle faults and joints within the Trans-Amazonian gneisses increases. Fault-bounded lenses of metagranites occur as tectonic slivers within schists of the Porongos group near the border faults associated with fractured quartz veins. The Trans-Amazonian basement thus was uplifted along steep faults. Despite the antiformal structure in map view and the dip of the Porongos sequence (NW-dipping in the northwestern part, SE-dipping in the southeastern part), the overall structure does not represent a broad open anticline. The rock units and specific layers of the Porongos group cannot be traced from northwest to southeast as would be the case if they represented the two limbs of a fold. Hence, the different lithological units of the Porongos sequence are exposed in the southeastern and northwestern parts of the Porongos belt. The southeastern parts comprise metapelitic schists with quartzites, marble lenses and acid metavolcanic rocks intercalated with graphite schists and banded iron formations (Jost & Bitencourt, 1980; Remus *et al.* 1987; Porcher & Fernandes, 1990; Remus, Hartmann & Ribeiro, 1991). The northwestern part consists of metapelites, quartzites with local intercalated conglomeratic beds, acid metavolcanics intercalated with felsic tuffitic rocks, and minor marble lenses and ultramafics.

Jost (1982) and Remus, Hartmann & Ribeiro (1991) mapped a metamorphic zoning from the chlorite zone to the garnet–staurolite zone from east to west also reflected by Al_2SiO_5 modifications (andalusite, kyanite).

Jost & Bitencourt (1980) subdivided the supracrustal rocks of the Porongos belt into an autochthonous unit (Grupo Cerro dos Madeiras) in the east and an allochthonous unit (Cerro da Árvore) which was transported to the west. More recent studies reject this subdivision, and due to intense overprinting of the original stratigraphy, relative age-relationships are unknown and the usage of previous stratigraphic terms should be avoided.

A strongly different view is presented by Porcher & Fernandes (1990). They interpret quartzites and quartzo-feldspathic rocks in the west as corresponding in large part to intensely mylonitized granitoids. Hence, in their opinion, the majority of the schists in the westernmost parts of the belt represent overprinted plutonic rather than metasedimentary and metavolcanic rocks.

The age of the supracrustal rocks is unknown. Conventional U–Pb ages of zircons from a meta-andesite in the Santana area give 783 ± 8 Ma (Chemale, 2000); a metarhyolite of the Capané region shows an age of 783 ± 6 Ma (SHRIMP) (Porcher *et al. in* Hartmann, Porcher & Remus, 2000). These data are interpreted as crystallization ages giving constraints on the approximate age of the metasedimentary rocks with which they are intercalated. Basei *et al.* (2000), however, propose that the age of the volcanism is not representative of the time of deposition of the metasedimentary units. They suggest that the data instead give the age of the metamorphic climax which led to anatexis of the deep levels of the sedimentary pile resulting in the observed volcanism. This would imply a pre-Neoproterozoic deposition of the sedimentary rocks.

The metavolcanic rocks are intercalated with the metasedimentary rocks. Tuffitic layers alternate with metapelites, arkoses and cherts. The metavolcanic and metasedimentary rocks record the same structural evolution. This favours the former interpretation that volcanism was coeval with sedimentation and thus, the 780 Ma crystallization ages of the intercalated metavolcanic rocks give the approximate age of deposition in the Porongos basin.

2.b. Geology of the Santana da Boa Vista region

The basement of the Santana da Boa Vista region is exposed in the core of the broad Santana antiform in the central parts of the belt (Figs 3, 4). It is made up

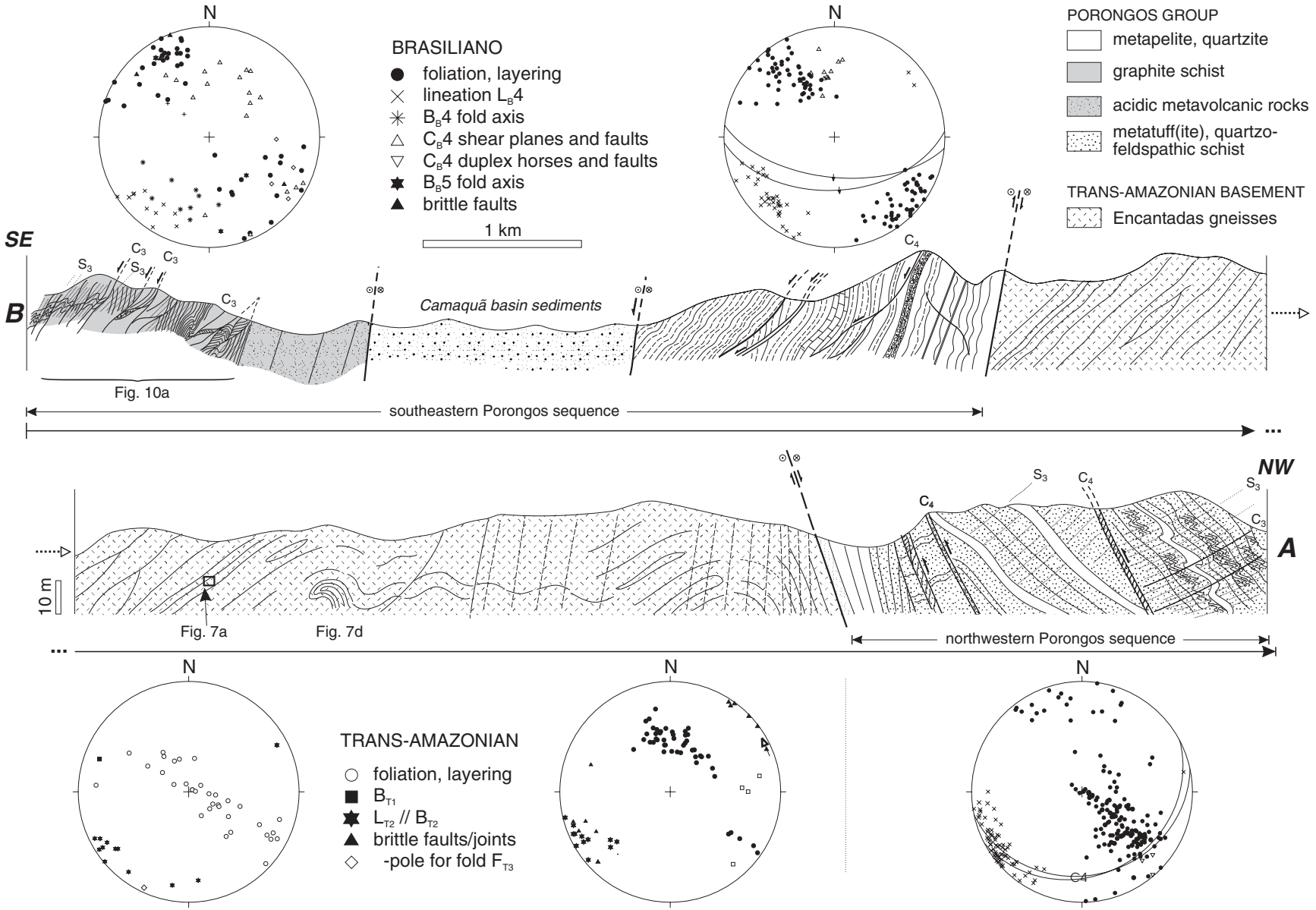

Figure 4. SE–NW-oriented geological section through the Santana da Boa Vista area (with supplements from Remus *et al.* 1990) and lower hemisphere stereoplots showing structural data of different segments. For section location see Figure 3.

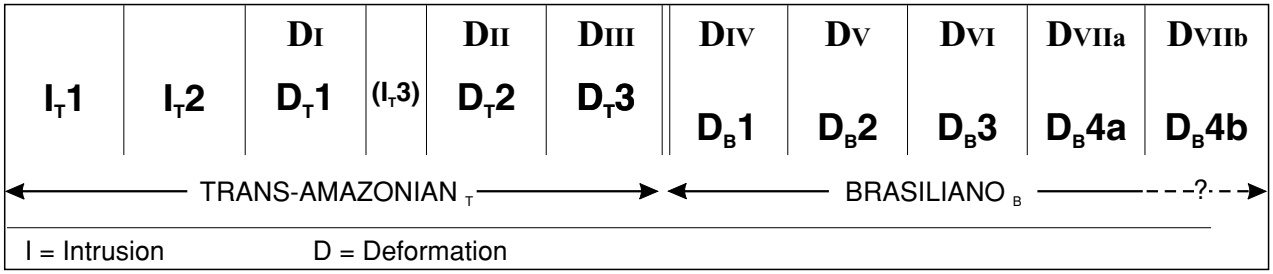

Figure 5. Number of deformational phases in the basement (Encantadas Complex) and metavolcano-metasedimentary Porongos sequence. DI to DIII can be assigned to the Palaeoproterozoic Trans-Amazonian orogeny and are labelled as D_T1 to D_T3. DIV to DVII occur in the Porongos sequence and thus belong to the Brasiliano orogeny and hence are labelled as D_B1 to D_B5.

of the Encantadas gneisses, local amphibolite lenses and mylonitized granites (Porcher & Fernandes, 1990; Remus *et al.* 1990). The amphibolites occur as NE–SW- to ENE–WSW-oriented stretched and boudinaged pods within the gneisses (Hartmann *et al.* 2003).

The volcano-sedimentary Porongos group in the eastern part of the Santana da Boa Vista section contains pelitic schists and graphite schists (Fig. 3) as well as acid metavolcanic rocks. The succession is cut by normal to oblique strike-slip faults of the narrow NE–SW-striking Piquiri Basin. To the west of this basin, a metapelite–quartzite succession is exposed including marble lenses (Fig. 4), and metarhyolites are exposed further north near Santana da Boa Vista town ('Passo da Ilha volcanics') (Fig. 3). Within the alternating metapelite–quartzite sequence, a trend of increasing grain size displayed by northwestward-decreasing thicknesses of metapelites, and northwestward-increasing portions of quartzite can be observed. Near the faulted contact to the basement the quartzites contain conglomeratic beds. The contact to the Encantadas gneisses which crop out in the core of the broad Santana anticline (Figs 3, 4) is marked by a brittle fault. To the west of the basement, the Porongos sequence consists of quartzites, metapelites, and intercalated quartzo-feldspathic rocks as well as some cherty beds which resemble banded iron formations. The quartzo-feldspathic rocks are interpreted as either meta-arkoses (Jost & Bitencourt, 1980; Remus, Hartmann & Ribeiro, 1991) or mylonitized granites (Porcher & Fernandes, 1990). These rocks are rich in feldspar, which occurs as porphyroclasts as well as in fine-grained layers. Some porphyroclasts have rounded shapes. Metamorphism and deformation occurred at greenschist-facies conditions with cataclastic deformation of feldspar. Some quartz pods are polycrystalline quartz pebbles resembling detrital resedimented components within these rocks. The rocks are therefore interpreted to represent metatuffitic rocks.

3. Structural evolution

Because of poorly known age data, especially from metamorphic minerals which could provide the age of deformation and related metamorphism, the age of the deformations in the basement gneisses is not clear, that is, whether the fabric, or parts of the fabric, of the Encantadas Complex are the result of Neoproterozoic Brasiliano overprint or the structures represent preserved Palaeoproterozoic (Trans-Amazonian) deformations. Therefore, the whole succession of deformational phases preserved in the Porongos belt, in both the basement and in the Porongos sequence, is numbered with Roman numerals from DI to DVII (Fig. 5). However, it is necessary to distinguish between deformations of the basement displaying possible pre-Brasiliano structures, and Neoproterozoic Brasiliano fabrics, also for reasons of correlation of some deformational phases which occur in both units. Hence, in the more detailed description of the deformations the phases are numbered with Latin numbers and labels, that is, deformation phases in the Trans-Amazonian basement are labelled with T and deformations proposed to be related to the Brasiliano orogeny are labelled with B (Fig. 5). Structures related to a deformational phase Dn are named Fn (folds), Sn (foliations), Cn (shear zones), etc.

Although a number of deformations (D1–Dn) can be distinguished and labelled, one should be aware that different phases, for example, superposed folding, do not necessarily represent temporally separated events but might be transitional and belong to one single deformation episode. D_B1 to D_B3, for example, might represent increments of one single deformation event reflecting progressive deformation at increasing metamorphic degree. Nevertheless, they represent distinct phases or steps of progressive deformation which can be distinguished by their structures. A designation of D1 to Dn is used in the sense that distinct deformation phases and related structures can be recognized and separated in terms of their fabrics, timing by overprinting relationships, kinematics, and sometimes metamorphic grade as well. It is not meant to indicate that single phases represent single orogenic events.

3.a. Structure of the Palaeoproterozoic basement

The tonalitic to granodioritic Encantadas orthogneisses show a well-developed compositional banding parallel

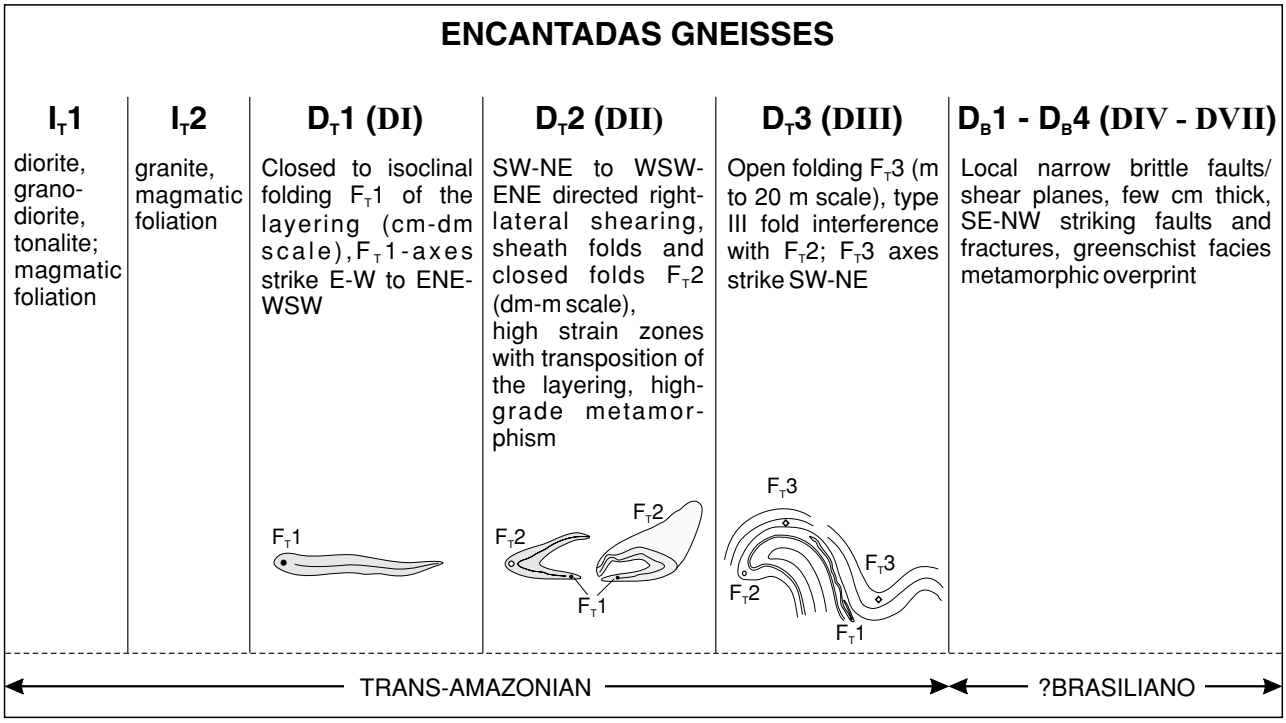

Figure 6. Overview of the sequence and characteristics of deformational phases preserved within the basement (Encantadas gneisses).

to the dominant foliation. The layering itself is intensely folded and comprises isoclinal folds parallel to the banding. Subsequent later folding led to formation of similar folds and sheath folds. The foliation is steeply inclined and in most cases the foliation planes dip 55–85° to the SSE or SE, in some places 85° to the NW. Various dips are attributed to NW-vergent folding which is supported by the occurrence of subordinate NW-vergent folds. Some gneisses show low-strain zones displaying a weak foliation and irregular open folding. They are alternating with high-strain zones which are characterized by a well-developed foliation parallel to the compositional banding due to transposition, rootless isoclinal folds and boudin formation. Synkinematic granitoids intruded subparallel to the foliation planes or, when intruding in high-strain zones, were rotated and transposed parallel to the shear zone foliation.

The foliation in the gneisses is defined by thin biotite and thick quartz–feldspar layers. Quartz forms lens-shaped aggregates rather than coherent layers. Their elongate shape is oriented parallel to the foliation. The quartz aggregates consist of medium to coarse grains with serrate grain boundaries as well as smaller isometric grains with low-energy grain boundaries. The quartz aggregates show a crystallographic preferred orientation. Plagioclase porphyroblasts in some gneiss samples have lobate grain boundaries and show patchy undulose extinction. The matrix is composed of fine-grained recrystallized feldspar.

Gneiss samples from higher-strain zones display a well-developed foliation defined by strong alignment of biotite as well as the elongate shape of quartz–feldspar aggregates.

Amphibolites occur as SW–NE-striking lenses (boudins) on a centimetric to decimetric scale. They represent mafic dykes which were boudinaged and stretched parallel to the dominant foliation. Some amphibolites represent monomineralic hornblendites; others contain layers of hornblende and plagioclase. Actinolite is also present in the samples. Some amphibole grains show a thin rim of probably different composition and are surrounded by epidote, suggesting a greenschist-facies retrograde overprint resulting in formation of actinolite and epidote.

3.a.1. Structural evolution

Detailed structural analysis establishes the following sequence of magmatic and deformational phases (Fig. 6).

The evolution started with the intrusion (I_T1) of diorites, granodiorites and tonalites, possibly as synkinematic plutons in a shear zone environment accompanied by formation of a magmatic foliation. A second phase of intrusions (I_T2) includes the emplacement of synkinematic granitoids. The gneisses show different degrees of deformation with high-strain zones displaying a well-developed foliation; other parts show a less-developed alignment of minerals and transposition of the layering. It is likely that the gneisses represent synkinematic intrusions in a magmatic arc environment (note tonalitic and granodioritic composition)

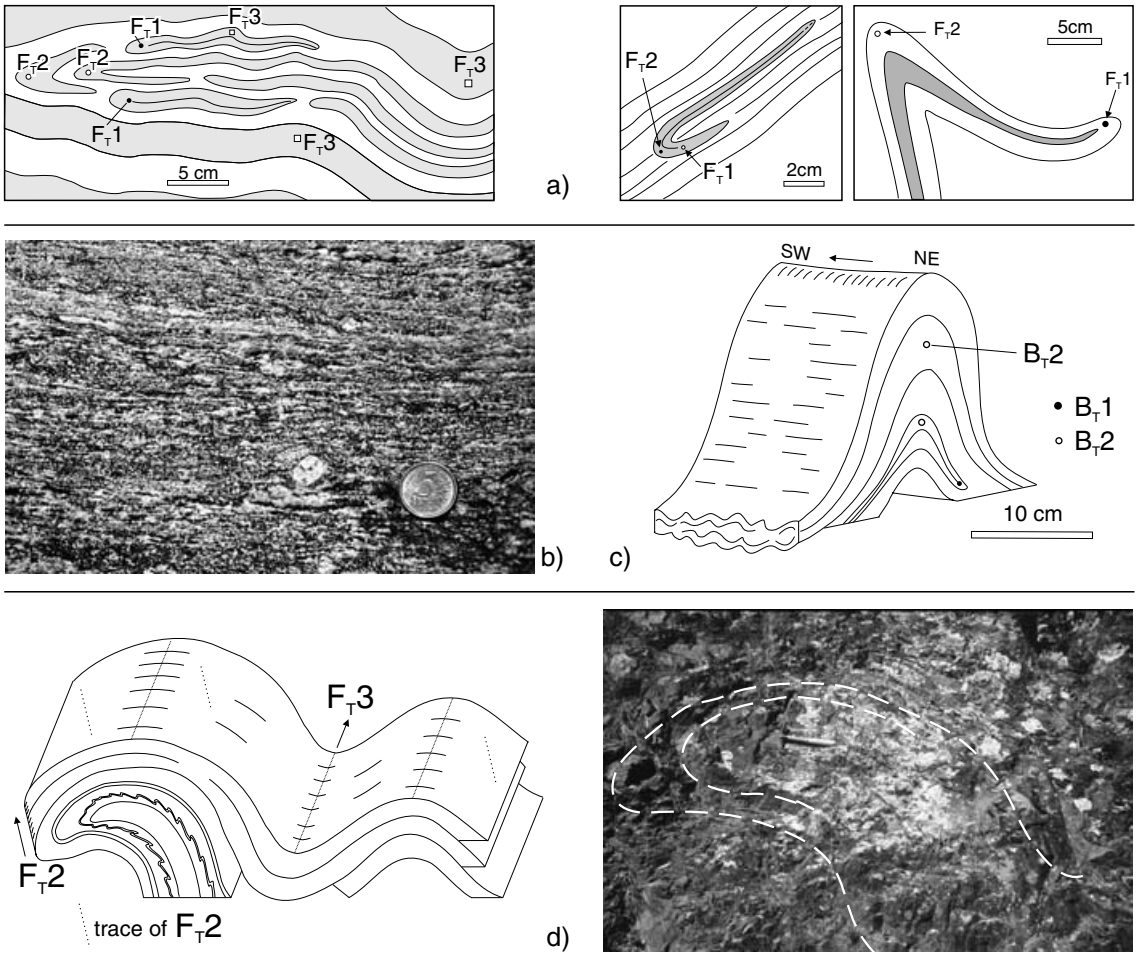

Figure 7. Detailed structures within the Palaeoproterozoic basement observable in outcrop scale. (a) Refolding of F_T1 folds during D_T2 closed and D_T3 open folding (location see Fig. 4); left = SE. (b) D_T2 high strain zone within the Encantadas gneisses at Passo da Moinho displaying σ-shaped feldspar porphyroblasts which indicate a dextral sense of shear; left = ENE; scale: coin diameter = 2 cm. (c) Refolding of F_T1 folds during D_T2 closed folding. (d) Fold interference pattern of SW–NE-striking F_T2 and SSW–NNE-oriented F_T3 folds at the BR-392 road cut near Santana da Boa Vista town; left = ESE; scale on photograph: hammer length = 32 cm.

so that their emplacement was accompanied by deformation.

During the first deformation D_T1 (DI) the layering was folded on a centimetric to decimetric scale (F_T1 folding). The fold axes of the closed to isoclinal folds strike E–W to ENE–WSW. Quartz–feldspar veins truncating the layering probably belong to a subsequent third plutonic event (I_T3). Isoclinal folds of quartz layers can also be observed in thin-sections.

The second deformation D_T2 (DII) is characterized by SW–NE- to WSW–ENE-directed shearing leading to the formation of similar folds (F_T2) on a decimetric to metric scale, transposition of the layering in high-strain zones, as well as refolding of the pre-existing F_T1 folds (Fig. 7a). Sheath folds are common at some localities. They formed by inhomogeneous simple shear that deformed the pre-existing F_T1 fold hinges so that they became curved within the fold axial surfaces. Low-strain zones show open to closed folding. The F_T2 fold axes strike SW–NE. ENE–WSW-oriented ductile shearing is indicated by σ-shaped feldspar porphyroblasts and asymmetric tails and pressure shadows (Fig. 7b). However, shear sense is not consistent. Many layers show a dextral sense of shear, whereas some others contain SC fabrics, asymmetric feldspar grains and quartz aggregates which favour a sinistral sense of shear. Nevertheless, right-lateral shearing seems to predominate. Some areas displaying higher strain show a pronounced SW–NE- to WSW–ENE-oriented stretching lineation L_T2 defined by elongated feldspar and quartz.

The third deformation D_T3 (DIII) is represented by open to closed folding on a scale of metres to tens of metres. Refolding of F_T2 by F_T3 folds can be observed in outcrops at the BR-392 road cut near Santana da Boa Vista town (Fig. 7d). The F_T3 fold axes strike SW–NE.

In contrast to ductile high-temperature deformations D_T1 to D_T3, the fourth deformation recognizable within the gneisses is represented by brittle to semi-brittle faults and shear planes, only a few centimetres thick, with SE–NW strike. Some SW- to SSW-dipping planes contain slickensides with a subhorizontal lineation

	Rock type	Metamorphic peak mineral assemblages	Retrograde minerals
PORONGOS sequence east	metapelite	ms (sericite) + qz + tourm ms (sericite) + qz + plag + hema + magn ± tourm	sericite
PORONGOS sequence west	metavolcanic rocks	qz + plag + czo + ms (sericite) + hema + magn ± bi ± chltd ± tourm	leuc, chl
	quartzite	qz + plag + ms (sericite) qz + plag + ms (sericite) + hema + magn ± tourm	
	metatuff(ite)	qz + plag + ms (sericite) + bi + hema ± tourm ± pyrite ± ep/czo ± chltd	sericite
	marble	cc + ms ± tremo ± ep	
ENCANTADAS Complex	tonalitic gneiss	plag +qz + bi + tourm + ti	chl; sericite
	gneiss	qz + plag ± microcline + bi + hbl + ti ± ep/czo ± tourm	leuc, hema, ep
	gneiss	qz + plag + ms ± microcline	hema, sericite
	porphyritic gneiss	qz + plag + bi + ti+ magn	
	amphibolite	hbl layer: hbl gneissic layer: hbl + plag	act act, ep, ti

act = actinolite; bi = biotite; cc = calcite; chl = chlorite; chltd = chloritoid; ep/czo = epidote/clinozoisite; hbl = hornblende; hema = hematite; leuc = leucoxene; magn = magnetite; ms = muscovite; plag = plagioclase; qz = quartz; ti = titanite; tremo = tremolite; tourm = tourmaline

Figure 8. Metamorphic mineral assemblages of the Porongos sequence and within the basement. In the Encantadas Complex, the mineral parageneses of $D_T2 + D_T3$ represent the peak metamorphic conditions of the Trans-Amazonian orogenic cycle, the retrograde assemblages formed due to a Brasiliano overprint. In the Porongos sequence, the metamorphic peak was associated with the Brasiliano deformations D_B1–D_B3. Retrograde minerals in these rocks formed during D_B4.

which indicates a NW–SE-oriented dextral sense of shear along these planes. Narrow millimetre-thick epidote veins are associated with brittle shear planes and faults. The brittle planes can possibly be linked with Brasiliano thrusting (D_B4, DVII) or brittle late-Brasiliano faulting (D_B5, DVIII) (see Section 3.b.4) and thus are interpreted as Brasiliano structures. In thin-sections, the gneisses are cut by narrow pressure solution seams and narrow cataclastic shear zones. These zones are characterized by brittle fracturing of feldspar, amphibole and large epidote grains as well as retrograde formation of fine-grained mica due to decomposition of feldspar. They might be linked with a Brasiliano overprint.

3.a.2. Metamorphic grade

The mineral assemblages of D_T1 and D_T2 in the gneisses (Fig. 8) represent the peak metamorphic conditions. Depending on their composition, they comprise quartz, plagioclase, ± microcline, hornblende, biotite, muscovite and tourmaline. The amphibolites consist mainly of hornblende. Grain boundary migration recrystallization of quartz occurs at high temperatures. Recrystallization of feldspar, which can be observed in the gneisses, starts at temperatures above *c.* 550 °C (Tullis & Yund, 1987). Some feldspar grains disintegrate to aggregates of fine-grained feldspar. Tourmaline has an olive green colour and shows no zoning suggesting diffusion which, according to G. Voll (unpub. Habilitation thesis, Univ. Berlin, 1969), indicates temperatures above 560 °C. Hence, amphibolite-facies metamorphic conditions can be inferred for the dominant deformations of the basement, D_T1 and D_T2.

Retrograde actinolite, epidote and titanite formation in the amphibolites indicate a greenschist-facies metamorphic overprint. Such an overprint can also be observed in the gneisses resulting in formation of

chlorite, sericite and leucoxene. This overprint could have occurred either during D_T3 or may be attributed to a Brasiliano overprint. Decomposition of feldspar to sericite can be linked with activity of cataclastic shear zones and fractures which are oblique to sub-orthogonal to the main foliation. They possibly belong to a Brasiliano overprint.

3.b. Structural evolution of the Porongos metavolcanic–sedimentary sequence

The dominant foliation of the metavolcanic–metasedimentary Porongos sequence dips mainly to the SE in the southeastern part of section, showing steeper dips as well as local NW-dipping planes in the central parts near the southeastern fault contact to the Encantadas gneisses, and dips to the NW in the northwestern part (Fig. 4). Although a first look might indicate a regional-scale anticlinal structure due to 'doming' of the gneisses, the real structural relationships are more complicated and the overall structure does not simply represent an open anticline.

The compositional layering of the metasedimentary rocks consists of already folded layers and thus represents a foliation rather than the primary layering. Due to isoclinal folding, this foliation could be parallel to the original bedding, however. This is also the case for the layering of the metavolcanic rocks sampled from Passo da Ilha, which also comprises isoclinal folds of quartz veins that were subsequently crenulated and refolded.

3.b.1. DB1

Quartz mobilizates and segregations forming during the first cleavage formation in metapelites serve as ideal markers for the reconstruction of the relative sequences of deformation phases (Nabholz & Voll, 1963). They form by pressure solution of quartz which then precipitates to form quartz mobilizates (Voll, 1960; G. Voll, unpub. Habilitation thesis, Univ. Berlin, 1969). These quartz veins occur parallel to the antithetic cleavage planes S1a which rotate into parallelism to S1 during progressive deformation. Once formed, the quartz mobilizates deform during subsequent deformations by folding and thus conserve the first and subsequent deformations (Nabholz & Voll, 1963).

In the Porongos sequence, quartz mobilizates occur in the metapelitic rocks as well as in the graphite schists. Particularly the latter contain abundant quartz mobilizates which were subsequently folded and refolded. Thus the formation of quartz mobilizates associated with a first foliation S_B1 (probably due to a first folding event) represents the first Brasiliano deformation D_B1 (Fig. 9).

The metamorphic temperatures during D_B1 can only be estimated. The formation of quartz mobilizates requires greenschist-facies conditions with temperatures above 280–300 °C (Voll, 1960).

3.b.2. D_B2 and D_B3

The layering and banding of the rocks consists of isoclinal folds on a scale of millimetres to centimetres. This is due to a second deformation phase D_B2 which caused isoclinal folding (F_B2) of S_B1 and the quartz mobilizates (Fig. 10a–c). The associated foliation S_B2 is parallel to S_B1. A NNE–SSW-trending lineation L_B2 is only locally preserved on some foliation planes. Later deformations obliterated and partly extinguished possible shear sense indicators so that the shear sense can hardly be determined. Recrystallized quartz grains in thin-sections parallel to L_B2 show a shape-preferred orientation oblique to the foliation and might indicate a top-to-the-NNE sense of shear during D_B2.

A subsequent phase of closed isoclinal folding, F_B3 associated with D_B3, can be identified with the help of quartz mobilizates showing a refolding of isoclinal F_B2 folds (note folded mica seams within some quartz mobilizates in the graphite schists in Fig. 10b). The fold axes of the centimetre- to decimetre-sized F_B3 folds strike SW–NE and gently dip to the SW. A stretching lineation L_B3 is defined by stretched feldspar and quartz. Closed F_B3 folding of the layering can also be observed in metarhyolites east of Santana da Boa Vista town. The layers as well as quartz aggregates consist of isoclinal F_B2 folds which were refolded during D_B3. Most isoclinal folds preserved in the schists, however, probably represent F_B2 folds.

Some layers show a mylonitic fabric with a well-developed foliation and σ-shaped feldspar or SC structures defined by mica, suggesting development of localized ductile shear zones during this phase. Shearing is not restricted to the mylonitic zones but very likely was linked with F_B3 folding. The structures have been overprinted by later deformations, especially D_B4, which produced structures that are in some parts sub-parallel to the D_B3 fabric. Feldspar porphyroclasts have been rotated during shearing and folding. Many mantled feldspar porphyroclasts within metarhyolites at Passo da Ilha are developed as Φ clasts. Some feldspar grains, however, show weakly developed asymmetric strain shadows (σ-type). Although the sense of shear is not consistent, most strain shadows indicate a top-to-the-SW dextral sense of shear. In the metasedimentary and metatuffitic rocks, feldspar porphyroclasts, locally developed SC fabric, a few occurrences of mica fish, as well as the development of a second foliation of recrystallized quartz grains arranged oblique to the main foliation in the shear zones in most cases, also indicate a top-to-the-SW directed dextral sense of shear.

In thin-sections, the quartz layers show a pronounced crystallographic preferred orientation. Dynamic re-crystallization is dominated by subgrain formation.

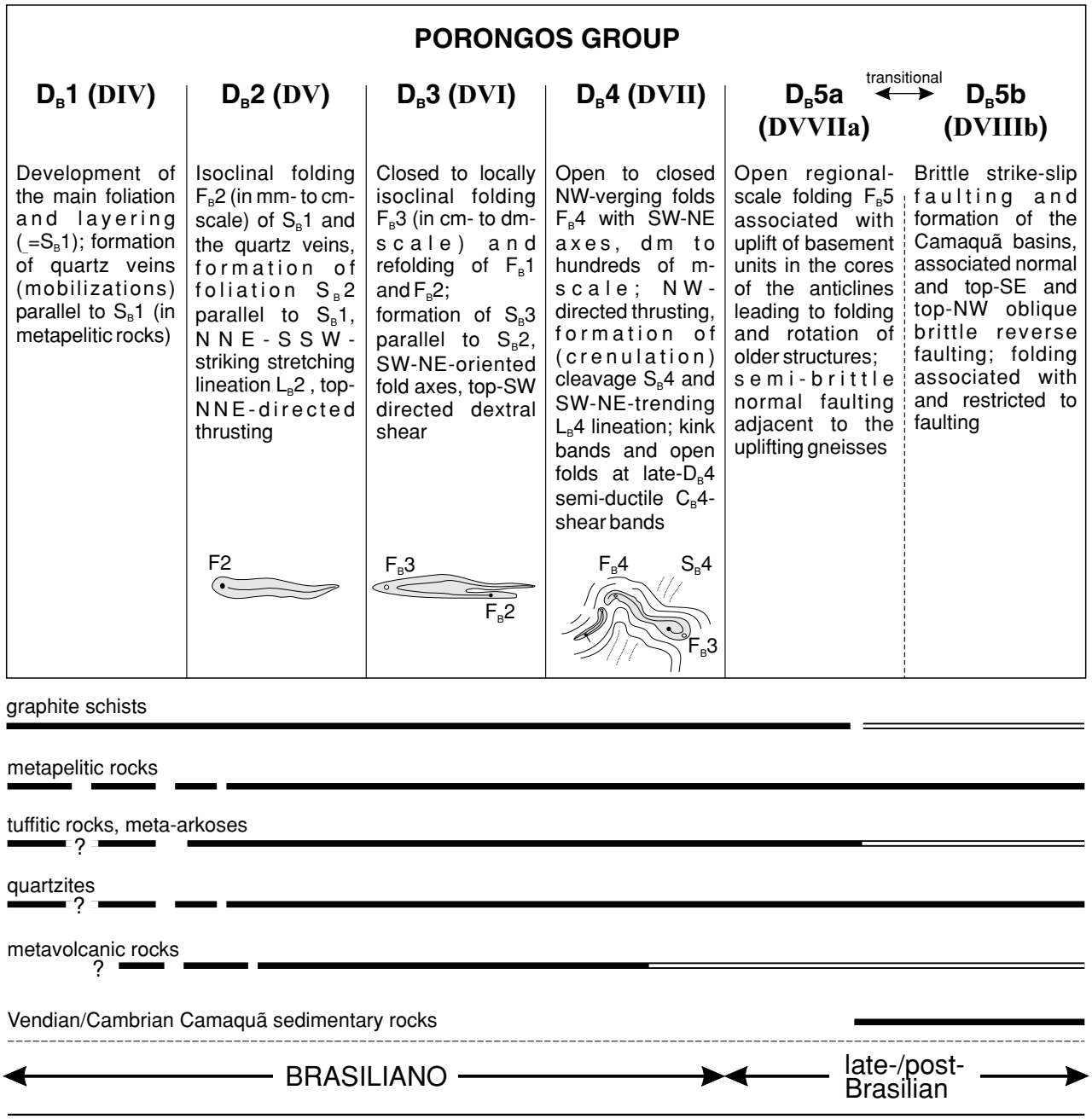

Figure 9. Overview of the sequence and characteristics of deformational phases in the Porongos sequence.

Few large crystals are transformed to ribbon grains. Recrystallized grains in most quartzite samples are more or less uniform in size. Most grains show a shape-preferred orientation parallel to the foliation in both sections cut parallel to the SW–NE-oriented L_B3 lineation (XZ) and in sections cut perpendicular to the lineation (YZ). However, in some domains, recrystallized grains form a second foliation oblique to the main foliation indicating a dextral sense of shear. In some samples, recrystallization occurs mainly at the grain boundaries and is characterized by sutured grain boundaries with bulges and small recrystallized grains which occur at the grain boundaries (bulging recrystallization *sensu* Stipp *et al.* 2002). The old grains show subgrain rotation recrystallization.

Subgrain rotation is also the dominant recrystallization process in the metapelitic and metatuffitic rocks. Many quartz layers and quartz mobilizates consist of recrystallized grains which define a new foliation arranged oblique to the external foliation, indicative of a dextral sense of shear. Some quartz domains in rocks of the northwestern Porongos group in addition are composed of grains with lobate boundaries characteristic of grain boundary migration recrystallization.

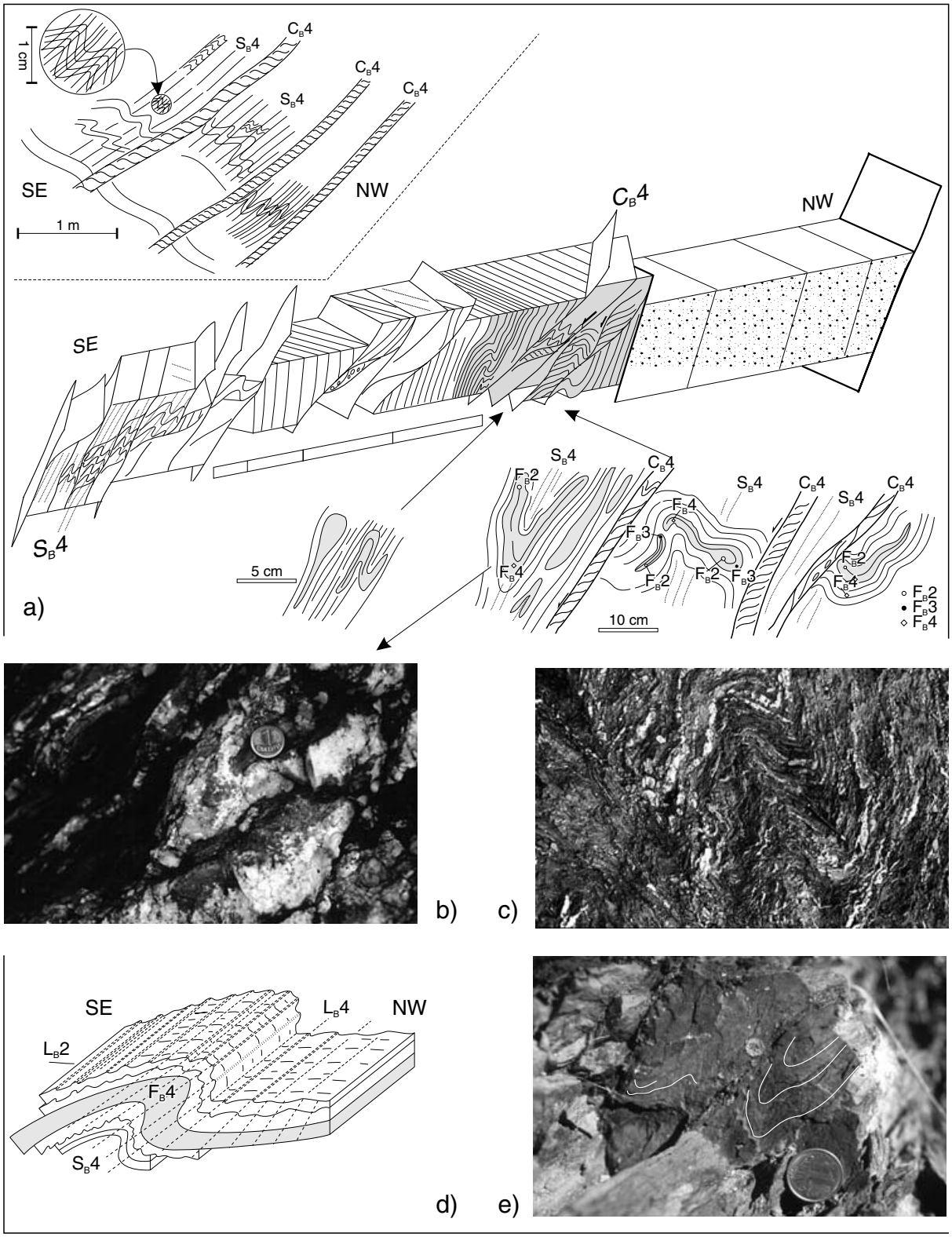

Figure 10. (a) Detailed sketch of the structures in the metapelites and graphite schists of the southeastern Porongos sequence (enlarged section of Fig. 4). Note polyphase folding and refolding of D_B1 quartz mobilizates within the Graphite schists (folded mica seam within the mobilizates represent relics of S_B1). Inlet illustrates crenulation and NW-vergent kink folding of metapelites in the northwestern Porongos sequence. Late C_B4 shear planes are oriented parallel to the S_B4 crenulation cleavage. (b) Refolded quartz mobilizates; left = SE; scale: coin diameter = 2 cm. (c) F_B4 folds within graphite schist related to C_B4 shear zones. Note refolding of pre-existing isoclinal folds defining the layering; left = SE; scale: pencil length = 12 cm. (d) NW-vergent F_B4 fold in metapelitic rocks of the southeastern Porongos sequence. L_B4 is a crenulation lineation parallel to the F_B4 fold axes. An older stretching lineation L_B2 is preserved on the foliation planes. (e) Closed F_B4 folding of metatuffitic rocks in the northwestern Porongos sequence; left = SE; scale: coin diameter = 2 cm.

D_B2 and D_B3 occurred during peak metamorphic conditions. The mineral assemblage of the metapelitic rocks in the eastern part of the Porongos belt (Fig. 8) comprises mainly quartz, plagioclase and sericitic muscovite; some rocks contain zoned tourmaline grains.

The mineral assemblages of metapelitic and metatuffitic rocks in the northwestern Porongos sequence contain biotite, muscovite, epidote/clinozoisite and local chloritoid (Fig. 8) suggesting upper greenschist-facies metamorphic conditions with temperatures above 400 °C. This is supported by the tremolite + epidote mineral assemblages of the marbles as well as by a biotite, chloritoid and clinozoisite/epidote assemblage in the metatuffitic rocks. The quartz fabric is typical for greenschist-facies conditions with temperature of 400–500 °C (Stipp *et al.* 2002); grain boundary migration recrystallization observed in some samples suggests higher temperatures and upper greenschist-facies conditions. The observed quartz fabric is compatible with the greenschist-facies assemblages. The metamorphic grade in the northwestern parts seems to be slightly higher than in the southeast.

3.b.3. D_B4

The fourth deformation, D_B4, is represented by open to closed folding on a scale of decimetres to hundreds of metres. In outcrop scale, D_B4 is characterized by crenulation of the layering and formation of decimetric- to metric-scale chevron folds in fine-grained rocks (Fig. 10c). Competent quartzite layers are folded to open NW-verging folds (Fig. 10d). The F_B4 fold axes strike SW–NE. The foliation S_B4 is a crenulation cleavage and generally dips gently to the SE, both in the southeast and northwest of the section. It is well developed in the metapelites, graphite schists and in the metavolcanic rocks. The decimetric- to metric-scale folds in the outcrops are subordinate folds to the large-scale (hundreds of metres) fold structures. Recumbent folds on a scale of several hundred metres, related to possible nappe transport, have been recognized by Remus *et al.* (1987).

A SW–NE-striking, mostly gently SW-dipping lineation, L_B4, frequently occurs on the foliation planes. It is parallel to the F_B4 fold axes and represents a crenulation lineation (Fig. 10d), whereas a stretching lineation, defined by stretched quartz, is only locally developed in quartzites. Kink bands and local folds are associated with narrow (centimetres to decimetres thick) semi-ductile shear zones (C_B4) (Fig. 10a) which are subparallel to the cleavage S_B4. These shear zones occur only in the metapelitic rocks (including the graphite schists). Penetrative D_B4 crenulation of the layering as well as small-scale folding and kink fold development can also be observed in the metarhyolites east of Sanatana da Boa Vista town. In localized high-strain shear zones which run parallel to the SW–NE-striking S_B4, the transposition of the pre-existing foliation is more intense and the folds are closer.

D_B4 post-dates the metamorphic climax and took place under retrograde conditions. Minerals like chlorite (at biotite) and leucoxene formed during D_B4 and indicate lower temperatures than during D_B2 and D_B3. The S_B3 foliation is overprinted by spaced S_B4 pressure solution seams which are common in thin-sections. Fine-grained sericite formed at S_B4 cleavage planes, whereas older and larger muscovite grains become bent or kinked.

The constant SE-dip of S_B4 in the northwest and southeast was associated with NW-vergent folding. Since the rocks of the metavolcanic–metasedimentary successions in the northwestern and southeastern parts of the Porongos belt represent two sequences or formations, they do not form the limbs of a large-scale anticline but instead relics of two distinct NW-vergent fold structures (on a scale of several hundred metres to a kilometre). Hence, D_B4 NW-vergent folding was probably associated with NW-directed thrusting (Fig. 11) leading to transport of the southeastern units of the Porongos sequence onto the northwestern parts. The thrusts truncated a pre-existing rock sequence with decreasing metamorphic grade to the top, formed during D_B2 and D_B3. The D_B4 thrust faults probably used the schist–basement contact as basal detachment.

The original contacts between the rock units in the southeastern and the northwestern parts in the Santana da Boa Vista area are not exposed due to later block faulting (see Section 3.b.4). It thus cannot be proved whether the contact is represented by a thrust fault as proposed (Fig. 11). NW-directed thrusting and fold nappes, however, can explain the general SE-dip of S_B4, as well as the occurrence of tectonically juxtaposed granite slices within the Porongos schists. These slices occur next to the contact fault of the Trans-Amazonian gneisses to the northwestern Porongos group. Although the original basement–schist contact probably represents the main detachment and thus thrusting was thin-skinned, tectonic slivers of the basement could have been incorporated due to splay faulting (Fig. 11). D_B4-related thrusting probably led to formation of a series of thrust sheets, comprising at least two major thrust units, resulting in a NW-vergent thrust stack which characterizes the overall geometry of the Porongos belt.

3.b.4. D_B5

The thrust stack was cut by semi-brittle to brittle faults during D_B5 (Fig. 11). D_B5 led to open regional-scale folding due to uplift of the gneisses (D_B5a), followed by faulting mainly along SW–NE-striking steep faults (D_B5b) so that the thrust stack was rotated and displaced by faults. The original nappe geometry was obliterated by block tectonics. The deposition of the oldest sedimentary successions of the Camaquã basin can be

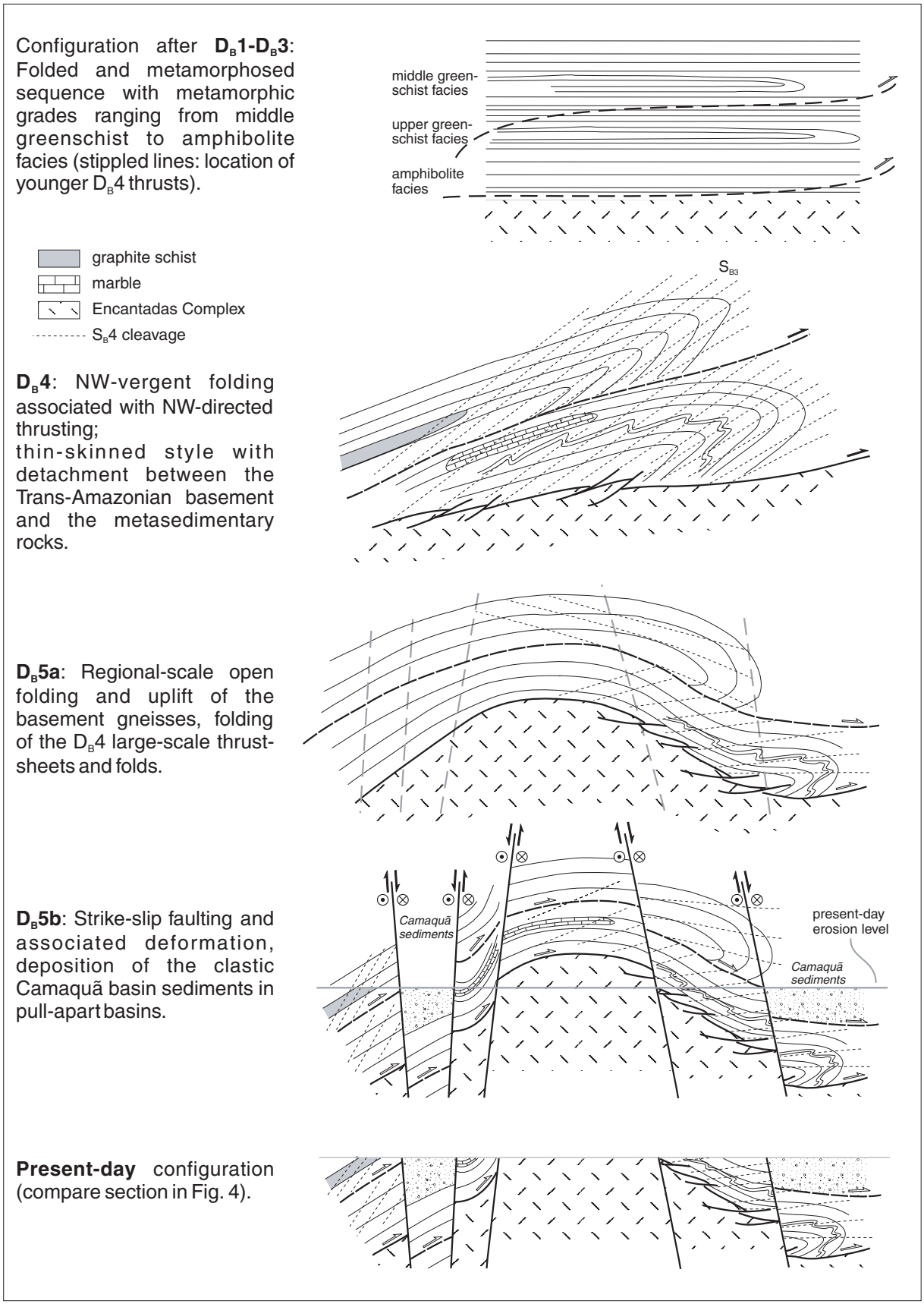

Figure 11. Schematic sketch (without scale) illustrating the NW-vergent folding and thrusting in the Porongos belt during D_B4 and subsequent block faulting leading to the present-day configuration. The scheme starts with the configuration after D_B1–D_B3.

assigned to this episode of faulting. Brittle faulting, development of fault-bounded basins, their narrow, elongate NE–SW-oriented shape and the relatively thick sedimentary fill suggest that the basins, at least the older ones, formed as pull-apart basins (e.g. the Piquiri basin in the eastern part of the Porongos belt in the Santana da Boa Vista area, see Fig. 3), during SW–NE-oriented left-lateral strike-slip. Top-to-the-SE and top-to-the-NW directed brittle oblique reverse faults cut the Porongos sequence, locally with development of small-scale duplex structures or formation of fault breccias and drag folding. The contemporaneous occurrence of strike-slip faults, oblique normal faulting in transtensional segments and oblique reverse faults in transpressional segments support an overall left-lateral strike-slip regime along SW–NE-striking major faults. Pressure solution seams forming localized SC shear bands observable in thin-sections, which indicate a sinistral top-to-the-NE directed shear sense, can likely be assigned to this deformation.

D_B5 took place in the late stages of the Brasiliano orogenic cycle. The deformed lower sequences of the Camaquã basin represent the first deposits of a molasse basin, and it is a common feature of mountain belts that basin development already begins during the late orogenic stages and the deposits thus could be affected by deformation as well.

4. Geochemistry

4.a. Samples and analytical procedures

Ten samples of metasedimentary and metavolcanic rocks have been analysed. The metavolcanic rocks comprise metarhyolites, from both the southeastern and northwestern part, and an acid metatuff from the northwestern sequence. Metasedimentary samples from the southeastern portion are represented by graphite schist and metapelite. Quartzite, metapelite and tuffite were sampled in the northwest.

For geochemical analyses (major and trace elements) whole rock samples of 5 to 10 kg have been crushed and powdered. Chemical analyses of major elements have been obtained by XRF (Bondar Clegg Laboratories, Canada), trace elements have been analysed with ICP-MS (Bondar Clegg Laboratories, Canada) or XRF (Geoscience Institute, Universidade Federal do Rio Grande do Sul, UFRGS, Porto Alegre).

For Nd analyses, whole rock samples were powdered and spiked with a 150Nd/149Sm spike prior to dissolution. The separation was performed in two steps including (1) cation exchange columns with HCl chemistry followed by (2) separation of Sm and Nd on teflon columns. Samples for Rb–Sr analyses were spiked with $^{85}Sr/^{87}Rb$ and separated by cation exchange columns. The mass spectrometer analyses were performed at the Isotopic Geology Laboratory of the Universidade Federal do Rio Grande do Sul (UFRGS), Porto Alegre, Brazil. Nd compositions were corrected to a value of 0.511856 for the La Jolla standard and fractionation corrected to $^{146}Nd/^{144}Nd = 0.7219$. Sr compositions are normalized to $^{86}Sr/^{88}Sr = 0.1194$. The results presented in Tables 3 and 4 are an average of ± 100 (Sm–Nd) and ± 130 (Rb–Sr) isotopic ratios per sample. The protolith ages (780 Ma) chosen for calculation of $\varepsilon Nd(t)$ are based on the 783 ± 6 Ma zircon age of an interbedded metarhyolite (U–Pb SHRIMP: Porcher *et al. in* Hartmann, Porcher & Remus, 2000).

4.b. Major and trace element data

The major and trace element analyses are listed in Tables 1 and 2. With the exception of one dacite sample (from the southeastern part of the Porongos belt), all metavolcanic protoliths are rhyolites. The metavolcanic rock samples have a subalkalic character.

Chondrite-normalized rare earth element (REE) patterns of all samples show high contents of incompatible elements, light REE (LREE) enrichment and depletion in heavy REE (HREE). The patterns of both the metasedimentary and metavolcanic rocks are similar to the patterns of upper continental crust with LREE enrichment and flat HREE patterns. The patterns of the quartzite samples are all similar in shape but compared to the other metasedimentary rocks they have lower abundances which could be attributed to a dilution by quartz. The mature sediments probably were derived from multiple recycling of old crust and older sediments and thus contain low contents of minerals other than quartz; in such lithologies the element concentrations are highly influenced by the element concentrations of heavy minerals.

In multi-element variation diagrams normalized to chondrite, the patterns match with the pattern of the Encantadas gneiss sample and both are similar to the pattern of the upper continental crust. They also fit well with patterns observed at Andean-type active continental margins except that they do not exhibit the concave HREE pattern. Again the patterns of the quartzite samples have nearly similar shapes but lower abundances. However, they also show highly variable values. The deviations in element contents of the quartzite samples are apparent in a spider diagram normalized to NASC (North American Shale Composite) (Fig. 12). Most metasedimentary samples show relatively flat patterns in contrast to two quartzite samples which exhibit strong depletion especially in large ion lithophile elements (LILE) like Rb, Ba, Th and Sr. They are thus depleted especially in mobile elements relative to the other rocks. This can be explained by secondary mobilization of these elements as they are prone to solution which might have occurred due to weathering (possibly already during sediment recycling processes also) or possible fluid flow during volcanism and/or deformation.

Table 1. Whole rock trace element analyses

Sample	Encantadas gneiss BR-140/2	Graphite schist BR-142/1	Dacite BR-143/1	Metapelite BR-144/1	Rhyolite BR-145/1	Quartzite BR-151/3	Quartzite BR-151/4	Rhyolitic tuff BR-152/1	Tuffite BR-152/2	Quartzite BR-156/1
Rb		84.42*		210.52*			243.34*	106.41*	61.18*	5.93*
Cu	16	64	26	55	23	3	28	9	12	2
Pb	14	21	16	25	31		13	8	3	
Zn	64	129	58	40	109	5	72	49	13	
Mo	2			4	1	2				1
Ni	26	54	35	13	25	6	41	9	8	3
Co	16	47	27	11	22		19	11	10	
Mn	452	783	1013	110	782	24	154	242	128	17
Ba	284	683	560	604	832	23	539	1153	1090	21
Cr	57	94	42	73	48	97	93	45	36	86
V	51	112	92	102	88	4	71	36	31	4
Sr	387	98	85	121.17*	159	8	60.15*	220	221	2
Y	10	20	27	12	27	7	18	16	6	
Ga	13	13	12	19			20	10	11	
Li	24	55	67	40	29	8	36	22	20	3
Nb	11	22	15	14	16		13	11	4.16*	
Ti	2900	6800	5000	4000	4800	100	4600	2500	2100	200
Zr	60	165	104	121	85	25	112	46	44	22
Ce	44	130	89	77	89	9			63	27
Eu	0.8	2.2	1.2	1.5	1.2				0.9	
La	20	64	43	38	42	12	46	36	36	20
Lu	0.1	0.7	0.6	0.6	0.4	0.1				
Nd	16	61	38	35	40	14	30.84**	25.83**	23	12
Sc	10	20.5	16.3	14.9	17.6	0.6	13		3.5	0.8
Sm	3.2	13.1	7.6	7.7	8	2.5	5.61**	4.49**	3.5	1.8
Tb		2	1	1	1					
Th	7.7	21	16	14	21	0.8	13.33*	20.13*	9.3	1.2
U		4	4	5	5					
Yb	1	5	4	4	3	1				
Hf	3.8	6.9	6	5.1	5.9	2	3.95*	4.8*	3.7	1.1

* = XRF; ** = mass spectrometry

Table 2. Whole rock major element analyses

Sample	BR-140/2	BR-143/1	BR-144/1	BR-145/1	BR-152/1	BR-152/2
SiO_2	65.50	64.03	65.56	63.41	69.76	69.91
TiO_2	0.49	0.82	1.22	0.78	0.40	0.34
Al_2O_3	16.43	16.34	15.69	14.51	13.93	15.15
Fe_2O_3	4.33	6.42	8.60	6.10	3.14	2.78
MnO	0.06	0.14	0.01	0.10	0.03	0.02
MgO	1.84	2.09	0.57	2.52	1.49	1.31
CaO	2.86	0.89	0.21	3.61	0.89	0.63
Na_2O	4.75	1.35	0.52	2.08	2.19	2.74
K_2O	2.15	3.83	3.56	3.41	6.03	3.99
P_2O_5	0.15	0.12	0.10	0.20	0.11	0.12
Cr_2O_3	0.02	0.01	0.02	0.02	< 0.01	< 0.01
Total	99.38	99.37	100.26	99.11	99.29	98.86

Compared to upper crustal values, the metavolcanic samples show a slight depletion in high field strength elements (HFSE) like Nb and Zr. A large negative Nb anomaly is absent. When normalized to MORB, the patterns of the metavolcanic samples exhibit strong enrichment in incompatible and LIL elements as well as LREE enrichment, whereas the HREE pattern is flat.

As Th and Sc are considered to be immobile, the Th/Sc ratio is an excellent provenance indicator (Taylor & McLennan, 1985). Th is a tracer for a felsic source and Sc is indicative of mafic source components. All samples show Th/Sc ratios of about 1, consistent with upper crustal derivation, or are > 1 which is characteristic for sediment recycling. This is compatible with the observation that the highest Th/Sc values occur in the quartzites and in a tuffitic rock. The high Th/Sc ratios of the samples implying low Sc concentrations indicate no considerable contributions from a mafic source. This is further supported by the fact that none of the sedimentary samples shows a significant enrichment in Cr since Cr is also indicative of a mafic source component. This is also true for the metavolcanic samples which show Cr concentrations similar to the metasedimentary rocks.

4.c. Sm–Nd and Rb–Sr data

Without exception, all samples show very evolved negative initial εNd(t) values and high depleted-mantle

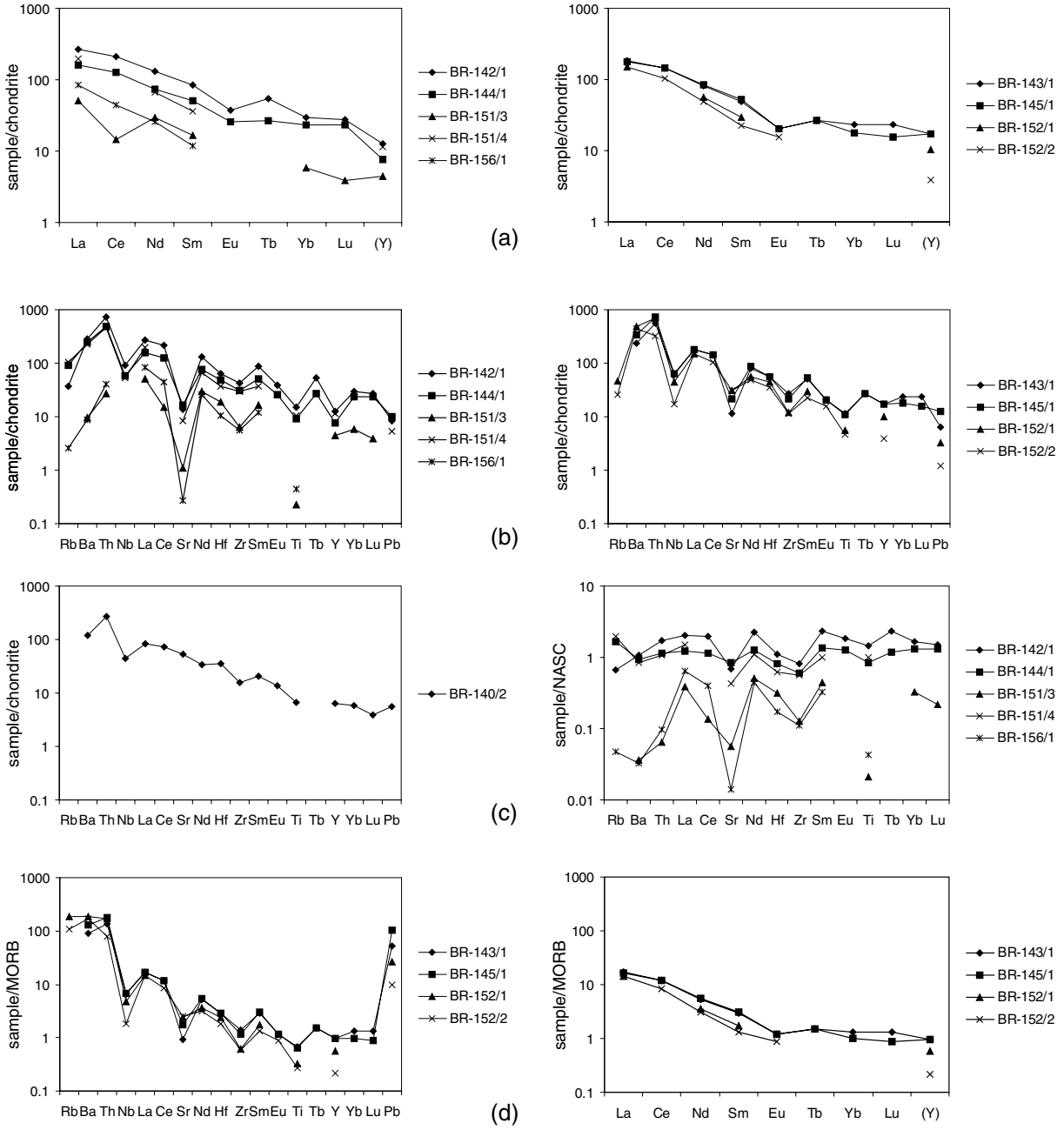

Figure 12. Rare Earth Element patterns as well as spider diagrams of different rocks of the Porongos sequence normalized to chondrite and N-MORB (normalizing values after Sun & McDonough, 1989). (a) Chondrite-normalized REE diagrams of metasedimentary rocks (left) and metavolcanic and metavolcanoclastic rocks (right). (b) Chondrite-normalized spider diagrams of metasedimentary rocks (left) and metavolcanic and metavolcanoclastic rocks (right). (c) Left: chondrite-normalized spider diagram of an Encantadas gneiss sample; right: spider diagram of the metasedimentary rock samples normalized to NASC (North American Shale Composite, normalization values after Gromet *et al.* 1984). (d) N-MORB-normalized multi-element (left) and REE diagrams (right) of the metavolcanic and metavoclanoclastic samples of the Porongos sequence.

model ages (TDM model ages) (Fig. 13). The εNd(t) values, calculated for an assumed depositional age of 780 Ma, are −6.25 and −6.85 for the metasedimentary rocks of the southeastern Porongos sequence; the metadacite sample shows a similar value of −6.87. The εNd(t) values of the metasedimentary rocks of the northwestern part of the section vary between −14.72 and −17.96, while the metavolcanic and metavolcanoclastic rocks show even lower values of −20.64 and −21.72 (Table 3). The samples from the southeastern part of the section show less evolved εNd(t) values and significantly lower TDM model ages between 1734 and 1954 Ma, compared to 2346–2710 Ma TDM model ages in the northwestern part (Table 3, Fig. 14). The two groups of TDM model ages suggest that the rocks of the northwestern and

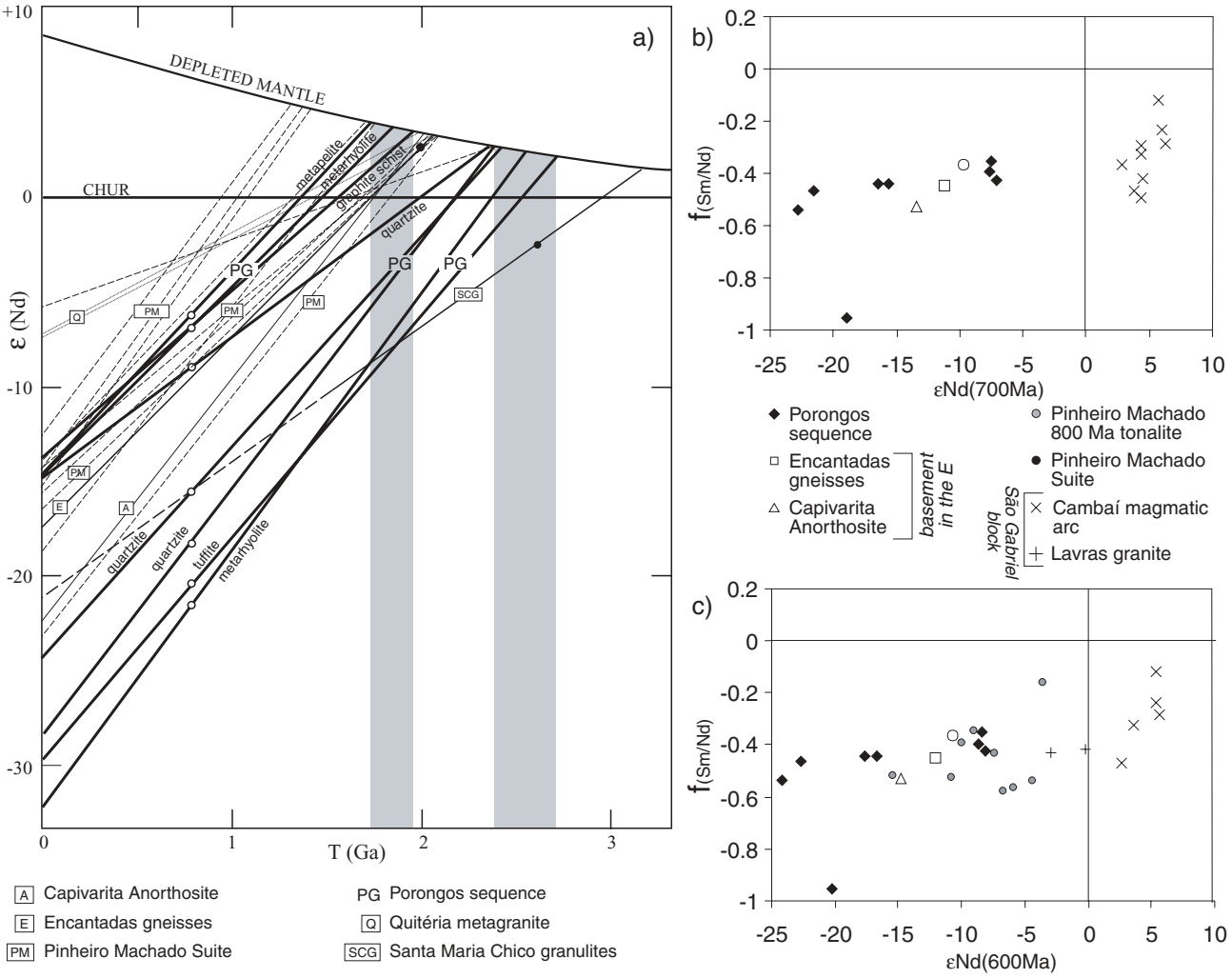

Figure 13. (a) Nd data for the São Gabriel block. The intersection with the model depleted mantle (DM) curve (DePaolo, 1981) give TDM ages (assuming no Sm–Nd fractionation) (CHUR = chondritic uniform reservoir). Shaded area outlines the two TDM model age groups of the Porongos sequence. Circles give the dated (black) or assumed (white) age for calculation of εNd(t). For comparison, Nd data of basement units as well as of the Pinheiro Machadi granitic suite are added (Santa Maria Chico granulites: Mantovani, Hawkesworth & Basei, 1987; Arroio dos Ratos/Encantadas gneiss recalculated from Silva *et al.* 1999; Capivarita Anorthosite: Silva *et al.* 1999; Pinheiro Machado Suite: Babinski *et al.* 1997; Silva *et al.* 1999; Quitéria metagranite: Koester *et al.* 1997). (b, c) f(Sm/Nd) v. εNd(700 Ma) and εNd(600 Ma), where f(Sm/Nd) = [(^{147}Sm/^{144}Nd)sample / 0.1967] – 1. Values for the Encantadas gneisses and Capivarita Anorthosite are calculated from data of Silva *et al.* (1999), Pinheiro Machadi Suite from data of Babinski *et al.* 1997 and Silva *et al.* 1999; data for the São Gabriel block are from Saalmann *et al.* (2005) except of the Lavras granite which was calculated from data of Babinski *et al.* (1996).

Table 3. Whole rock Sm–Nd isotopic data

Sample	Sm (ppm)	Nd (ppm)	^{147}Sm/^{144}Nd	^{143}Nd/^{144}Nd	Error (ppm)	εNd(0)	Age (Ma)	εNd(t)	TDM (Ma)
BR-142/1	4.07	19.26	0.127758	0.511935	18	−13.72	780	−6.85	1954
BR-143/1	6.71	34.10	0.119039	0.511889	15	−14.60	780	−6.87	1846
BR-144/1	7.19	38.42	0.113075	0.511891	16	−14.58	780	−6.25	1734
BR-151/3	1.31	7.18	0.109937	0.511441	18	−23.35	780	−14.72	2346
BR-151/4	5.61	30.84	0.109963	0.511394	11	−29.26	780	−15.64	2417
BR-152/1	4.49	25.83	0.105165	0.511114	14	−29.73	780	−20.64	2710
BR-152/2	3.28	21.87	0.090761	0.510985	14	−32.25	780	−21.72	2547
BR-156/1	1.43	8.99	0.096379	0.501121	16	−27.94	780	−17.96	2380

Average of ± 100 isotopic ratios, 1.0 V of ionic intensity to the ^{146}Nd and multicollection with ^{146}Nd in the axial collector.
Normalization of ^{146}Nd/^{144}Nd = 0.7219 and fitted to the bias using Nd SPEX, with suggested ^{143}Nd/^{144}Nd = 0,511110 and caliBRated against Nd La Jolla standard using a value of ^{143}Nd/^{144}Nd of 0.511856; (^{143}Nd/^{144}Nd)$_{DM}$ = 0.51315; εNd(t) was calculated using (^{143}Nd/^{144}Nd)$_{CHUR}$ = 0.50663, (^{147}Sm = 6.54 × 10^{-12} and (^{147}Sm/^{144}Nd)$_0$ = 0.1967, and (^{143}Nd/^{144}Nd)$_0$ = 0.512638, respectively.

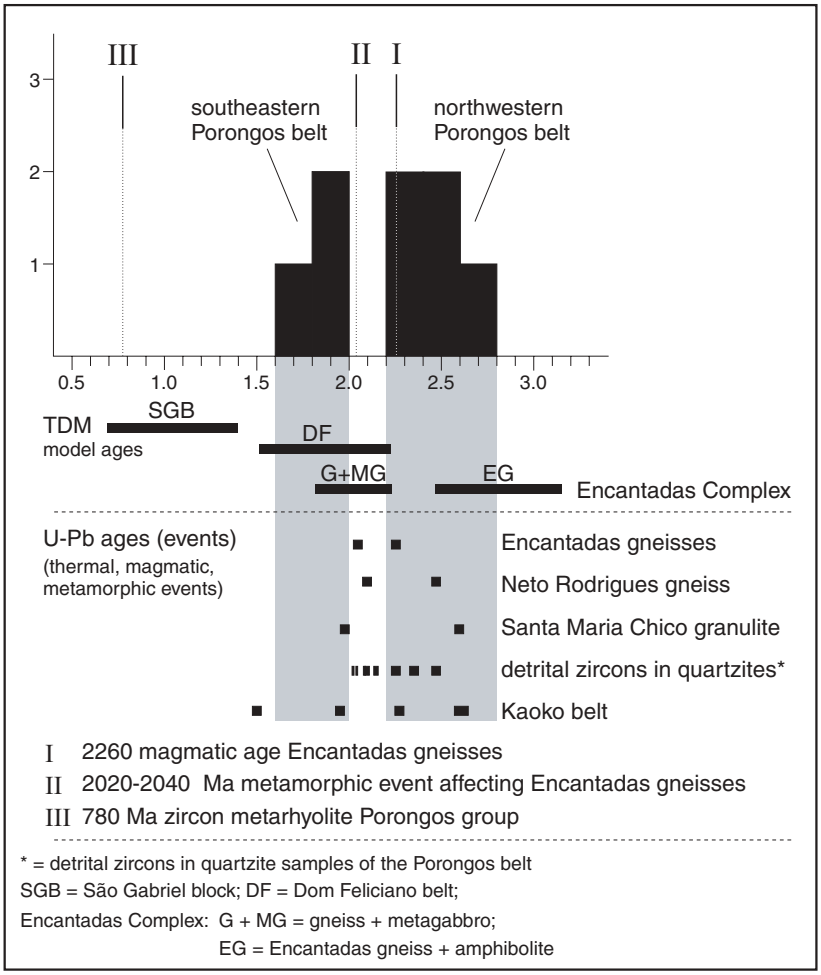

Figure 14. Frequency histogram of TDM model ages of the Porongos sequence. Two age groups reflect the distinction between a southeastern and a northwestern unit. The TDM model age ranges partially overlap with ranges for the Encantadas gneisses and for the Dom Feliciano belt (Encantadas gneisses: TDM model ages from Chemale, 2000; U–Pb ages from Hartmann, Porcher & Remus, 2000 and Hartmann *et al.* 2000; TDM model ages Dom Feliciano belt from Frantz *et al.* 1999; U–Pb data of Santa Maria Chico granulite from Hartmann *et al.* 1999; U–Pb data of Neto Rodrigues gneiss from Hartmann *et al.* 2000; detrital zircon U–Pb data for quartzites of the Porongos belt from Hartmann *et al.* 2004; U–Pb data of events in the Kaoko belt from Seth *et al.* 1998).

southeastern Porongos sequence could have been derived from different sources.

The basement units of the Porongos belt, that is, the Encantadas Complex, formed 2.2–2.0 Ga ago during the Trans-Amazonian orogeny (Babinski *et al.* 1997; Leite *et al.* 1998, 2000; Silva *et al.* 1999). Two groups of TDM model ages of the Encantadas Complex have been reported by Chemale (2000): the Encantadas gneisses and amphibolites have Archaean TDM model ages between 2.47 and 3.14 Ga; gneisses and metagabbros show Palaeoproterozoic model ages between 1.81 and 2.22 Ga, partially tying up with the magmatic ages of the Encantadas Complex (Fig. 14). The first group partly overlaps with the TDM model ages of the northwestern Porongos sequence. Hence the Encantadas gneisses very likely represent the main source rocks for the northwestern Porongos units. In addition, sediment supply derived from younger rocks caused the slight shift to younger TDM model ages of the northwestern Porongos sequence.

The TDM model ages of Brasiliano granites within the Dom Feliciano belt, which show significant contamination by old crust, range between 1.53 and 2.27 Ga (Frantz *et al.* 1999) and clearly overlap with the model ages in the southeastern Porongos sequence (Fig. 14), suggesting the same basement source for both rock units. This source might in part be represented by the gneisses and metagabbros of the younger age group of the Encantadas Complex.

Hartmann *et al.* (2004) present detrital zircon U–Pb data for quartzite samples of the Porongos belt obtained by SHRIMP. The authors identified several age peaks which they assign to possible source rocks of the region. The data support the Nd data of this study indicating that the Neto Rodrigues gneiss and Encantadas Complex are important source rocks of the Porongos sequence (Fig. 14).

A diagram plotting f(Sm/Nd) v. εNd(700 Ma) (Fig. 13) emphasizes the stratigraphical distinction of the northwestern and southeastern Porongos sequences.

Table 4. Whole rock Rb–Sr isotopic data

Sample	Rb (ppm)	Sr (ppm)	Rb/Sr	$^{87}Rb/^{86}Sr$	Error (SD abs)	$^{87}Sr/^{86}Sr$ (present)	Error (SD abs)	Age	$^{87}Sr/^{86}Sr(t)$
BR-142/1	84.00	91.00	0.92	2.6072710	0.260727	0.7576292	0.000800	780	0.7286
BR-143/1	175.37	127.06	1.38	4.0371414	0.002873	0.7558276	0.000096	780	0.7109
BR-144/1	212.00	114.00	1.86	5.2526600	0.525266	0.7630550	0.002900	780	0.7046
BR-151/3	8.13	3.07	2.65	7.7740995	0.008958	0.7929475	0.000336	780	0.7064
BR151/4	158.00	45.17	3.50	10.2974967	0.020542	0.8246118	0.000609	780	0.7099
BR-152/1	183.76	106.00	1.73	1.6293080	0.162930	0.7425314	0.000224	780	0.7244
BR-152/2	61.00	237.00	0.26	0.7269922	0.072699	0.7233738	0.000800	780	0.7153
BR-156/1	5.27	0.99	5.33	15.7787760	0.020439	0.8550230	0.000455	780	0.6793

Samples in *italic* = igneous samples; others = metasedimentary rocks.
Average of ± 130 isotopic values, 1.0 V of ionic intensity for ^{88}Sr and multicollector with ^{86}Sr in the axial collector.
Analyses of sample and standard solutions consist of ± 130 total ratios; the average measured $^{87}Sr/^{86}Sr$ ratio for the NBS-987 standard was 0.71026 ± 11. Normalization to $^{86}Sr/^{88}Sr = 0.1194$, fitted to bias with base on the $SrCO_3$ NBS-987, using $^{87}Sr/^{86}Sr = 0.71025$ and correction in order of the presence of spike. NBS values during analyses were 0.71026 ± 11. Initial $^{87}Sr/^{86}Sr$ values have been calculated by using the formula: $(^{87}Sr/^{86}Sr)t = (^{87}Sr/^{86}Sr)_{measured} - ^{87}Rb/^{86}Sr(e^{\lambda \times t} - 1)$, where t = proposed or measured age of the rock, $\lambda = 1.42 \times 10^{-11}$.

The northwestern Porongos rock samples plot at more negative εNd(t) values, even to the left of the Encantadas gneisses and the Capivarita anorthosite which constitute the basement in this area. They thus were derived from older source rocks not exposed in this area today.

The southeastern samples plot next to and slightly to the right of the basement rocks, suggesting that the Encantadas gneisses represent the dominant source of the metasedimentary rocks in the southeast. The slight shift to the right indicates input of detritus derived from younger source rocks. However, the rocks still display strongly negative εNd(t) values so that a considerable input from a juvenile source is unlikely. The juvenile Cambaí gneisses of the São Gabriel block in the west of the Southern Brazilian Shield are of approximately the same age as the Porongos sequence. However, metasedimentary rocks associated with the gneisses are clearly derived from the juvenile magmatic arc (Saalmann *et al.* 2005), in contrast to the metasedimentary rocks of the Porongos sequence. This makes a significant contribution from the juvenile magmatic arc in the west unlikely. Detritus may also have been shed from mafic volcanic rocks, intercalated with the Porongos sequence, which could explain the shift to younger sources.

In the same diagram, however, plotted for t = 600 Ma (Fig. 13), the samples of the southeastern Porongos sequence overlap with the values for the *c.* 610 Ma Pinheiro Machado magmatic suite (Silva *et al.* 1999) exposed in the Dom Feliciano belt to the east of the Porongos belt. The suite comprises K-rich granitic gneisses and the rocks show similarly evolved εNd(t) (−5.6 to −10) (Babinski *et al.* 1997), indicating that the magma must have been strongly contaminated by old continental crust. As the basement of this suite consists of the Encantadas gneisses, they represent the most probable contaminants. This is supported by the diagram where the rocks of the Pinheiro Machado suite plot next to or overlap with the Encantadas gneiss sample.

Sediment supply derived from old crust is also supported by Rb–Sr analyses (Table 4). The $(^{87}Sr/^{86}Sr)t$ values of the metasedimentary rocks, calculated for the supposed depositional age of t = 780 Ma, vary between 0.7064 and 0.7286, except for a metapelite which shows a lower value of 0.7046. The 0.6793 value of a quartzite sample (BR-165/1) is unrealistic. This could be result of disturbance of the Rb–Sr system in these rocks. On the other hand, it could be explained by a younger depositional age for this rock, as a calculation of $(^{87}Sr/^{86}Sr)t$ for t = 670 Ma, for example, gives a value of 0.7042. No distinction between samples from the northwestern and southeastern parts of the section is discernible. High values suggest contribution of an old source or reworking of older sediments and corroborate the Sm–Nd data.

The metavolcanic rocks exhibit high $(^{87}Sr/^{86}Sr)t$ values of 0.7190 and 0.7124 as well; sample BR-152/2 has a higher value of 0.7153 indicating a supply of sediment detritus, supporting its proposed tuffitic origin. The data confirm the interpretation of partial melting of, or considerable contamination by, old continental crust during magma generation and evolution.

5. Discussion and conclusions

5.a. Trans-Amazonian versus Brasiliano deformation

Although a Neoproterozoic depositional age for the Porongos sequence cannot be proven, a Neoproterozoic (Brasiliano) age of the deformations D_B1 to D_B5 is supported by the 783 ± 6 Ma U–Pb age of zircons from a metarhyolite (Porcher *et al. in* Hartmann, Porcher & Remus, 2000). If this age either represents the magmatic crystallization age (Porcher *et al. in* Hartmann, Porcher & Remus, 2000) and thus the approximate depositional age of the interbedded metasedimentary rocks, or the age of metamorphic climax as suggested by Basei *et al.* (2000), deformation and metamorphism is younger than or coeval with the *c.* 780 Ma age, respectively, and thus belongs to the Neoproterozoic Brasiliano orogeny.

The D_T1 to D_T3 deformations observed in the Encantadas gneisses cannot be simply correlated with

D_B1 and subsequent deformations in the Porongos sequence. Widespread high-temperature ductile WSW–ENE-oriented shearing during D_T2, for example, including a strong component of inhomogeneous shear and large values of shear strain (required for sheath fold formation) cannot be simply linked with D_B2 folding in the Porongos sequence.

The basement rocks were deformed at significantly higher metamorphic grade. Zircon SHRIMP studies in amphibolite samples suggest hornblende formation and metamorphic overprint near 2.0 Ga (Hartmann *et al.* 2003), related to the Trans-Amazonian orogeny. Metamorphsim was accompanied by deformation (D_T1–D_T3). It is thus suggested here that D_T1–D_T3 can be attributed to the Palaeoproterozoic Trans-Amazonian orogeny rather than to the Brasiliano orogeny. A long extrapolation of the discordia gives a lower intercept age of about 700 Ma, which can be interpreted as a result of activity of the Brasiliano orogeny (Hartmann *et al.* 2003), causing the formation of greenschist-facies mineral assemblages observed in the rocks. Retrograde greenschist-facies mineral formation, brittle shear planes and joints linked with the fourth deformation in the Encantadas gneisses, could be related to a Brasiliano overprint which, however, was localized and did not obliterate the dominant Trans-Amazonian fabrics.

5.b. Provenance and source rocks

The trace element (e.g. Th/Sc ratios) and Sm–Nd as well as Rb–Sr geochemical data of the Porongos sequence indicate reworking of old continental crust. The derivation from or contamination with crustal material explains the observed similarity of the multi-element patterns to typical upper continental crust.

The Sm–Nd data exhibit Palaeoproterozoic to late Archaean TDM model ages as well as strongly negative εNd(t) values for both metasedimentary and metavolcanic rocks. The data indicate provenance of the metasediments from old sources, that is, Palaeoproterozoic to Archaean basement units, and only a minor contribution from younger sources. Parts of the sediment supply may have been derived also from reworked sediments, which is consistent with observed Th/Sc values of > 1 in some samples. The Encantadas gneiss sample (br-40/1) has a Th/Sc ratio of only 0.77 and thus cannot represent the only source. Therefore, the metasedimentary rocks are derived from mixed sources including basement units and recycled sediments. The two TDM model age groups suggest either different contributions from younger source rocks or that different basement units contributed to the northwestern and southeastern sediments of the Porongos sequence. This could be due to different source areas and/or different directions of sediment transport (e.g. debris supply from the west and from the east). It could also reflect a different age of deposition of the northwestern and southeastern portions and associated different levels of erosion resulting in a change of exposed basement source units with time. It should be kept in mind, however, that only a small number of samples could be analysed so that this study is preliminary in nature.

The isotopic data exhibit evolved εNd(t) values, Palaeoproterozoic to Archaean TDM model ages and high initial $^{87}Sr/^{86}Sr$ values, which suggests that the melts of the rhyolitic to dacitic metavolcanic rocks formed due to partial melting of or significant contamination by old crust, whereas there is no sign of significant contribution from Neoproterozoic juvenile material. Hence, geochemical data indicate that these rocks, as highly influenced by older rocks, probably have inherited great parts of the geochemical signatures of the basement. The interpretation of tectonic settings with the help of discrimination diagrams based on geochemical signatures therefore might be questionable and must be used with care because they show the setting of the source rather than that of the Neoproterozoic lavas. The Sm–Nd data of the Porongos sequence, at least of samples from the eastern parts, have striking similarities with the signature of the Pinheiro Machado magmatic suite in the Dom Feliciano belt (Fig. 13), indicating the contribution of the same basement units.

Provenance investigations using detrital zircon U–Pb SHRIMP age dating for six quartzite samples of the Porongos sequence point to a derivation from Palaeoproterozoic (2488–1998 Ma) sources; the youngest zircons have ages of about 1998 ± 15 Ma (Hartmann *et al.* 2004). The detritus was shed mainly from the underlying Encantadas Complex with contribution from other rocks in the Shield like the 2.48 Ga Neto Rodrigues gneiss, for example (Hartmann *et al.* 2004) (Fig. 14). The TDM model ages of this study, however, indicate significant contribution also from Archaean sources older than 2.48 Ga. Mature sediments like quartzites contain almost entirely magmatic zircons so that the metamorphic sources remain undetected (Hartmann & Santos, 2004).

Taking this into consideration, it is interesting to note that zircon age peaks and the range of TDM model ages in the Porongos sequence also partially tie up with U–Pb zircon ages of magmatic and thermal events in the Kaoko belt reported by Seth *et al.* (1998) (Fig. 14). The older TDM model age group corresponds well to 2.58–2.65 Ga magmatic rocks in the South African counterpart, and the younger age group ties up with 1.9–1.7 Ga major igneous activity and granitoid magmatism. The Kaoko belt also contains 1.5 Ga old orthogneisses (Seth *et al.* 1998), which might also have contributed to the sediment supply and would have caused a shift of the TDM model ages of the eastern Porongos sequence to lower values. On the other hand, it cannot be ruled out that TDM model ages

younger than 2.0 Ga might be an artefact of Nd isotopic geochemistry since the quartzites contain no zircons younger than 1998 Ma (Hartmann *et al.* 2004). Note that sedimentary rocks represent a mixture of a number of source rocks and hence, TDM model ages give mixed ages depending on the relative contribution from these sources. This in many cases prevents a correlation with certain source rocks.

Nevertheless, the data may indicate a close spatial relationship of the basement areas of the Porongos belt, Dom Feliciano belt and Kaoko belt in Palaeo- and Mesoproterozoic times. Future studies are necessary to test this hypothesis.

5.c. Tectonic setting

The tectonic setting of the Porongis belt is ambiguous. This is also the case for its relationship to the neighbouring tectonostratigraphic units in the west (São Gabriel block) and east (Dom Feliciano belt). Different tectonic settings have been proposed for the Porongos belt, ranging from a passive margin (Jost & Bitencourt, 1980) to a back-arc position (Fernandes, Tommasi & Porcher, 1992; Fernandes *et al.* 1995; Babinski *et al.* 1997; Hartmann *et al.* 1999; Chemale, 2000; Hartmann *et al.* 2000) or even a forearc setting (Issler, 1983).

The São Gabriel block comprises juvenile Neoproterozoic tonalitic and dioritic orthogneisses (Koppe & Hartmann, 1988; Chemale, Hartmann & da Silva, 1995; Babinski *et al.* 1996; Hartmann *et al.* 1999) and an associated Neoproterozoic volcano-sedimentary succession (Saalmann *et al.* 2005; Saalmann, Remus & Hartmann, 2005). Voluminous granite intrusions in the Dom Feliciano belt have also been interpreted as being linked with a magmatic arc setting (Fernandes, Tommasi & Porcher, 1992; Chemale, 2000). Hence, the Porongos belt would be located between two Neoproterozoic magmatic arcs. However, a magmatic arc setting for the Dom Feliciano belt is controversial since juvenile rocks are restricted to the São Gabriel block.

The Nd analyses of the metavolcanic and metasedimentary rocks clearly show reworking of the basement, indicating that the depositional basin formed on continental crust. The Porongos belt could have formed: (1) in an ensialic back-arc basin to the west of the Dom Feliciano belt, assuming that the Dom Feliciano belt represents a magmatic arc (Fernandes, Tommasi & Porcher, 1992; Fernandes *et al.* 1995; Chemale, 2000); (2) in an ensialic back-arc basin to the east of the magmatic arc located in the São Gabriel block; or (3) in a rift setting associated with a passive margin environment.

A back-arc basin environment of the Porongos belt to the west of the Dom Feliciano belt would imply a more or less contemporaneous magmatic activity in both areas and coeval sediment deposition in the back-arc region. The major magmatic and tectonic events in the Dom Feliciano belt, however, occurred between 630 and 600 Ma (e.g. Hartmann *et al.* 1999; Silva *et al.* 1999; Philipp, Nardi & Bitencourt, 2000; Leite *et al.* 2000), in some parts starting already at about 670–650 Ma in the Dorsal de Canguçu Shear Zone (Koester *et al.* 1997; Fernandes & Koester, 1999). Assuming a *c.* 780 Ma depositional age for the Porongos sequence (see Section 2.a), deposition took place prior to the proposed arc development and magmatism in the Dom Feliciano belt, which contradicts a back-arc tectonic setting for the basin.

The 780 Ma age of volcanism in the Porongos belt fits well with a basin development in the back-arc position of the 800–700 Ma magmatic arc in the São Gabriel block. However, Neoproterozoic metavolcanic rocks, as well as metasedimentary deposits in the São Gabriel block associated with the magmatic arc, have positive εNd(t) values and are clearly derived from juvenile source rocks (Saalmann, Remus & Hartmann, 2005; Saalmann *et al.* 2005). Isotopic signatures of the metavolcanic and metasedimentary rocks of the Porongos group in contrast do not show indications for a significant contribution of a Neoproterozoic juvenile source, nor have detrital zircons with ages below 1989 Ma years been recorded. It is unlikely that the sedimentary rocks deposited in the western portions of a magmatic arc or active continental margin are clearly derived from the juvenile igneous rocks, whereas no debris was shed to the back-arc basin in the east. This is especially unlikely since andesitic metavolcanic and metavolcaniclastic rocks, which are interpreted as volcanic parts of the magmatic arc (Koppe & Hartmann, 1988; Chemale, Hartmann & da Silva, 1995; Babinski *et al.* 1996; Hartmann *et al.* 1999, 2000), are exposed near the border of the two belts. This area therefore marks the boundary between predominantly juvenile rocks in the west (São Gabriel block) and reworked old continental crust in the east (Porongos belt and Dom Feliciano belt) and thus probably represents a tectonic boundary of two distinct tectonic blocks. Hence, a back-arc basin setting for the Porongos belt seems unlikely.

Zircon SHRIMP data from quartzites of the Porongos sequence (Hartmann *et al.* 2004) indicate a provenance which is entirely related to Palaeoproterozoic igneous rocks with only minor contribution from an Archaean source. The absence of Neoproterozoic zircons (Hartmann *et al.* 2004) leads to the conclusion that the Porongos basin formed on cratonized continental crust prior to the exposition of Neoproterozoic plutonic rocks. This is compatible with a passive margin or continental rift tectonic setting for the Porongos belt. The basin fill comprises mainly siliciclastic metasedimentary rocks, intercalated with metavolcanic rocks. The southeastern sequence consists of quartzites with subordinate conglomeratic beds passing to a quartzite–metapelite succession with increasing thickness of

metapelitic portions. This succession could represent a fining-upward sequence due to subsidence of the shelf if preserved in the original stratigraphic order. Basin formation occurred on stretched and thinned continental crust in an extensional (possibly transtensional) regime and deposition was accompanied by volcanism. A rift setting is also supported by the occurrence of interbedded alkali-rich theoleiites which have an age of about 880 Ma (Rb–Sr: E. Soliani, unpub. Ph.D. thesis, Univ. São Paulo, 1986) and are interpreted to represent rift-related rocks (Frantz & Botelho, 2000; Frantz *et al.* 2000).

A passive margin or continental rift environment is compatible with both deposition of shallow marine to deep shelf siliciclastic sediments with intercalated marble and stretching of continental crust leading to volcanism which is characterized by significant contamination by old continental crust.

The Porongos and Dom Feliciano belts share the same basement (Encantadas Complex). In the Dom Feliciano belt, deeper parts of the crust are exposed today. Although the main magmatism in the Dom Feliciano belt occurred in the period between 630 and 600 Ma, possible early granitoid emplacement is indicated by SHRIMP analyses of zircons of a tonalite xenolith which show a *c.* 700–800 Ma partial resetting of 2.1 Ga old zircons (Silva *et al.* 1999; Leite *et al.* 2000). About 800 Ma Rb–Sr whole rock analyses of calc-alkaline granitoids exhibit flat-lying mylonitic high-temperature solid state deformation (Frantz & Botelho, 2000). These rocks are coeval with deposition and volcanism in the Porongos basin. However, these rocks were derived from remobilization of Palaeoproterozoic crust (Babisnki *et al.* 1997; Leite *et al.* 2000) and therefore, the Rb–Sr whole rock ages very likely represent mixed ages. Many xenoliths occur in the granites of the Pinheiro Machado Intrusive Suite, which has an age of about 610 Ma (Babinski *et al.* 1997; Silva *et al.* 1999). This suite shows flat-lying shear zones which have been interpreted to be associated with convergent tectonics and ductile nappe stacking (Silva *et al.* 1999; Frantz & Botelho, 2000; Leite *et al.* 2000). However, the age, regional extent and tectonic meaning of this low-angle shear zone development are unknown. The flat-lying fabrics of the boudinaged xenoliths could also have formed coevally with the fabrics of the granite host, at about 610 Ma. Moreover, the 800 Ma resetting of the zircons represents the age of a thermal event rather than the deformation of the rocks. In other words, a proposed 800–780 Ma thermal overprint is not necessarily associated with convergent tectonics and ductile nappe stacking, since flat-lying fabrics are not necessarily related to collision but could also form in extensional regimes. Therefore, the 800–780 Ma resetting of zircon xenocrysts could also reflect partial melting of the basement due to crustal thinning as result of extension and stretching. This would be approximately coeval with basin formation, deposition and volcanism in the Porongos belt, and both were caused by stretching and thinning of the continental crust.

5.d. Age of the Brasiliano deformations and plate tectonic model

The juvenile São Gabriel block in the west contains relics of two magmatic arc assemblages, whereas the Porongos and Dom Feliciano belts are located on the Encantadas block and are characterized by reworking of old continental crust. The two tectono-stratigraphic blocks, or terranes, show a different structural and tectonic evolution until collision of the passive margin of the Encantadas block with the active continental margin in the São Gabriel block.

No age data exist for the Neoproterozoic deformation of the Porongos sequence. If deposition took place at about 780 Ma, associated with continental extension within the Encantadas block, D_B1 to D_B4 are younger than 780 Ma. Deposition in the Porongos basin occurred contemporaneously with westward subduction of oceanic crust of the São Gabriel/Goiás ocean beneath an active continental margin in the São Gabriel block in the west (Saalmann *et al.* 2005; Saalmann, Remus & Hartmann, in press) (Fig. 15a), where intrusion of the 750–700 Ma juvenile arc diorites, tonalites and trondhjemites occurred in localized zones of dextral shear during oblique oceanic plate subduction (Saalmann, 2004).

A change from extensional to collisional tectonics in the Porongos belt might be linked with the collision of the Encantadas block and São Gabriel block at about 700 Ma or shortly after 700 Ma (Fig. 15b). Collision caused SE-vergent thrusting in the São Gabriel block (upper plate) and isoclinal folding, shearing and metamorphism in the Porongos belt located on the lower plate (D_B1–D_B3). Late tectonic granites in the São Gabriel block indicate contribution from old continental crust in the juvenile block for the first time by showing slightly negative εNd(t) values (Saalmann *et al.* 2005).

The beginning of SW–NE-oriented sinistral transcurrent shearing along the Dorsal de Canguçu Shear Zone at the eastern border of the Porongos belt is marked by *c.* 670 Ma granite intrusions and shearing; synkinematic granite emplacement occurred until *c.* 617 Ma (Koester *et al.* 1997). While the granites probably intruded in transtensional segments of the shear zone (Fernandes & Koester, 1999), transpression could have caused large-scale NW-vergent folding and thrusting in the neighbouring Porongos belt corresponding to D_B4. NW–SE compression is compatible with contemporaneous left-lateral displacement in the SW–NE-oriented Dorsal de Canguçu shear zone. U–Pb SHRIMP analyses of zircons from an Encantadas gneiss sample located in the western Dom Feliciano

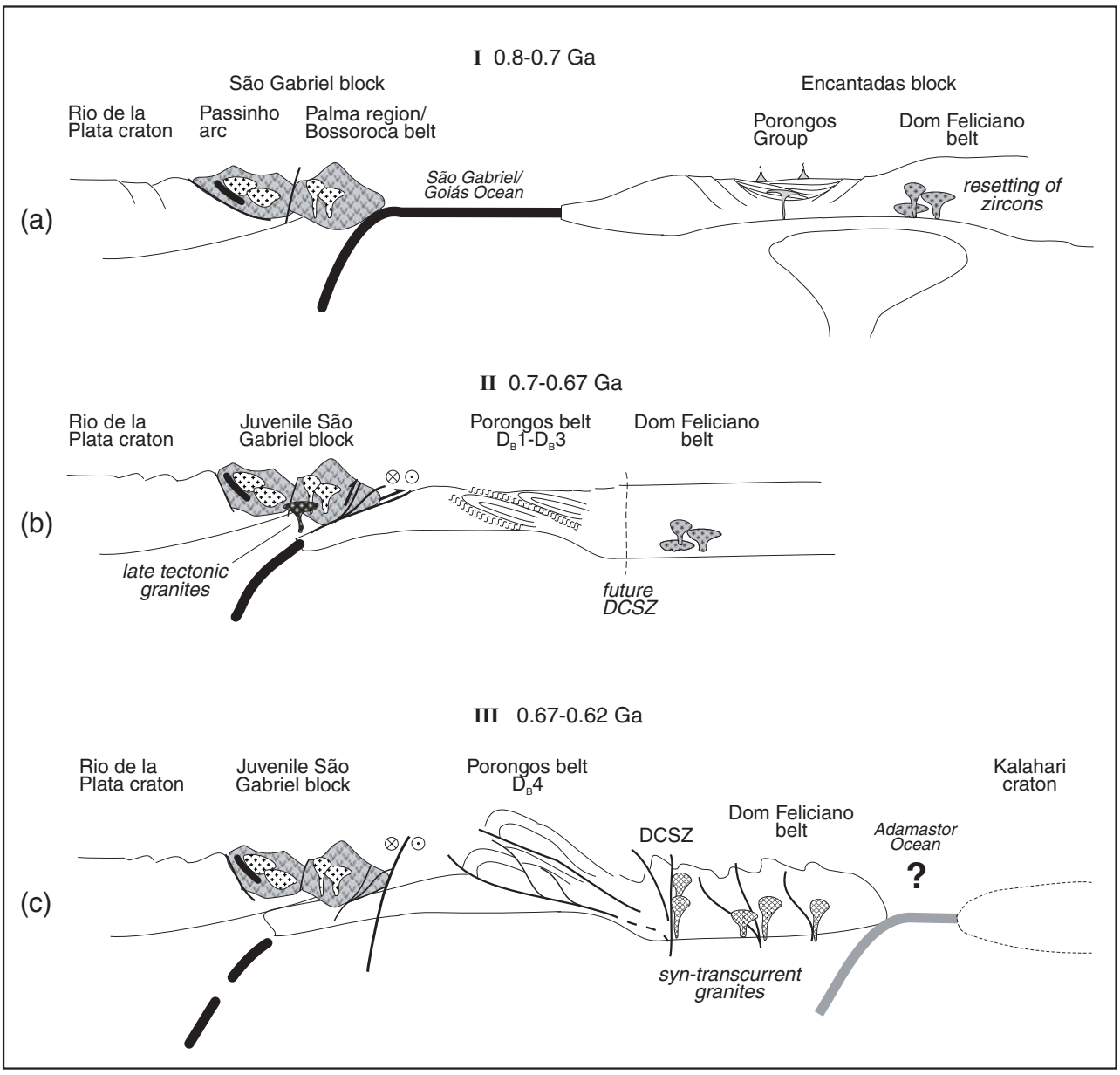

Figure 15. Plate tectonic model for the Brasiliano evolution of the Porongos belt. (a) Stage I: Basin formation on stretched continental crust in a passive margin environment. The continental crust was either part of the Kalahari or Congo craton or represents an independent microcontinent (Encantadas block) of ambiguous origin. Deposition of the Porongos sequence was accompanied by syndepositional volcanic activity due to advanced heat flow caused by thinning of the crust. Stretching and thinning of the continental crust leads to partial melting of the continental crust and resetting of zircons (possibly associated with first pulses of pluton emplacement) in the Dom Feliciano belt further east. At the same time, oceanic crust (São Gabriel or Goiás Ocean) is subducted to the west beneath the São Gabriel block which, at this time, represents the eastern active continental margin of the Rio de la Plata craton. Subduction caused accretion of juvenile crust in this area. (b) Stage II: Collision of the São Gabriel and Encantadas blocks, isoclinal folding and metamorphic overprint of the Porongos sequence (D_B1 to D_B3). (c) Stage III: Reconfiguration of the tectonic regime; activation of the transcurrent Dorsal de Canguçu Shear Zone (DCSZ) and D_B4 NW-directed thrusting and folding, syn-transcurrent granite emplacement is wide-spread in the DCSZ and in the Dom Feliciano belt. This might be linked to subduction of the Adamastor Ocean to the west beneath the Dom Feliciano belt; however, a magmatic arc environment of this belt is a subject of controversy.

belt near the border to the Porongos belt show a metamorphic overprint of 630 ± 13 Ma (Silva *et al.* 1999), which overlaps with the age of deformation and metamorphism in the Porongos belt.

Coeval transcurrent shearing and syntectonic granite intrusions are also widespread in the Dom Feliciano belt (Frantz & Nardi, 1992; Philipp *et al.* 1993; Babinski *et al.* 1997). This broad zone of transcurrent shear possibly was linked with late-collisional left-lateral movements compensating continuing convergence of the blocks (e.g. by lateral escape). This is supported by the fact that sinistral strike-slip also

occurred in the Porongos belt when nappe tectonics were followed by brittle D_B5 strike-slip faulting. Alternatively, shearing and granite magmatism might have been caused by subduction of the Adamastor ocean beneath the Dom Feliciano belt, so that the Encantadas block was located between a block in the west consisting of the Rio de la Plata craton and the accreted São Gabriel block and a subduction zone in the east (Fig. 15c). In this case the Encantadas block would represent a single microcontinent sandwiched between the Rio de la Plata and the Kalahari cratons in response to the closure of two oceans (Adamastor and São Gabriel/Goiás oceans). However, as stated above, a magmatic arc environment for the Dom Feliciano belt is still disputed and therefore marked with a question mark in Figure 15.

Brittle sinistral strike-slip faulting D_B5 in the Porongos belt occurred partly contemporaneously with 630–600 Ma ductile sinistral strike-slip shearing and synkinematic granite intrusions in the Dom Feliciano belt further to the east (Frantz & Nardi, 1992; Philipp *et al.* 1993; Babinski *et al.* 1997; Leite *et al.* 2000). The formation of the Camaquã sedimentary basins is related to this strike-slip faulting event (D_B5b) (Fig. 15d). The deposition and deformation of the Maricá Allogroup, which represents the sedimentary fill of the basins within the eastern Porongos belt (Piquiri and Arroio Boicí subbasins; see Figs 2, 3), is thought to have occurred between 630 and 600 Ma (Paim, Chemale & Lopes, 2000). This would imply a more or less continuous evolution from 670–640/630 Ma D_B4 thrusting and folding, associated with greenschist-facies metamorphism, to brittle D_B5 faulting and basin formation. The Guaritas subbasin in the northwestern Porongos belt contains the 592–580 Ma Bom Jardim Allogroup which is deformed as well (Paim, Chemale & Lopes, 2000). The lower, deformed succession of the Camaquã basin is overlain by an undeformed upper sediment pile. The intrusion of syntectonic granites like the 560–540 Ma Caçapava granite (Remus *et al.* 2000*b*) and the *c.* 540 Ma São Sepé granite (Chemale, 2000) demonstrate that strike-slip faulting occurred over a long time span, lasting at least until 540 Ma.

5.e. Regional implications

The Nd isotopic data suggest that detritus was shed mainly from the Encantadas Complex. The data support detrital zircon studies of quartzite samples of the Porongos belt by Hartmann *et al.* (2004), obtained by SHRIMP geochronology. The age peaks of the zircon populations are similar to detrital zircon data from the Brusque Complex in Santa Catarina 400 km further north and suggest that both belts are coeval (Hartmann *et al.* 2004). Moreover, the basement of the Brusque Complex in Santa Catarina can be correlated with the Encantadas Complex in the Porongos belt. Hence, both belts may have formed a continuous basin.

The Lavalleja group in Uruguay is located in the southern continuation of the Porongos belt. It also comprises a Neoproterozoic metavolcano-metasedimentary succession containing shales, arkoses, limestones and greywackes intercalated with mafic to felsic volcanic rocks (Sánchez Bettucci, Cosarinsky & Ramos, 2001). However, the basin is interpreted by these authors to have been formed in a back-arc tectonic setting, based on the geochemistry of igneous rocks within the succession. This argues against continuity between this belt and the Porongos sequence and Brusque Complex in southern Brazil. Moreover, according to Gaucher, Chiglino & Peçoits (2003), the units in Uruguay were not located between two cratonic blocks, namely the Rio de la Plata craton and a magmatic arc in the east (Dom Feliciano belt and equivalents).

In the Brusque and Porongos groups, zircon grains derived from Archaean source rocks are scarce, suggesting that Archaean cratons in Brazil (Santa Catarina Granulite Complex) and Uruguay (La China and Las Tetas complexes) and in southwestern and western Africa were either not exposed or located far away (Hartmann *et al.* 2004). Instead, the basin fill was derived from local Palaeoproterozoic sources. Hartmann *et al.* (2004) suggest the existence of a long continuous Palaeoproterozoic belt which formed from the Tandilia Belt in Argentina in the south to Uruguay (Piedra Alta Terrane) and southern Brazil (Arroio dos Ratos Complex) to Santa Catarina (Camboriú Complex) in the north. This belt would form the basement (and main source) of the Meso- to Neoproterozoic Porongos, Brusque and equivalent basins and would represent the basement of several continental blocks or microcontinents occurring in the Neoproterozoic belts in southern Brazil, that is, the Encantadas block and the Luis Alvez block. The Cuchilla Dionisio terrane in Uruguay may have been part of this belt since Nd model ages suggest an African affinity (Bossi & Gaucher, 2004). However, the basement of this terrane shows both Trans-Amazonian as well as Kibaran (Grenvillian) ages (Bossi & Gaucher, 2004), whereas the latter are absent in basement complexes in southern Brazil. As result of Meso-/Neoproterozoic rifting, the Trans-Amazonian belt possibly was fragmented into several smaller microcontinents or continental slivers which were subsequently amalgamated to the South American cratons during the Brasiliano orogenic cycle.

The origin of the Encantadas block, forming the basement of the Porongos and Dom Feliciano belts, is ambiguous. The microcontinent might have drifted away from Africa (the Kalahari or Congo craton) and subsequently attached to the Rio de la Plata craton. Palaeoproterozoic gneisses of the Dom Feliciano belt have been correlated with the Epupa Complex north and south of the Kaoko belt of southwest Africa (Leite *et al.* 2000). This would support an origin of

the Encantadas block from the Congo craton. The absence of Grenville rocks in the Encantadas Complex also argues against a connection with the Kalahari craton, since the 1.2–1.0 Ga Namaquã belt represents the basement of the Gariep belt. Alternatively, the Encantadas block previously was part of the Rio de la Plata craton and became detached and separated from it by opening of the São Gabriel/Goiás Ocean at *c.* 900 Ma. Future work including the study of isotopic tracers is needed to unravel the origin of this and other basement blocks in southern Brazil and Uruguay.

The main orogenic events in southern Brazil occurred between 880 and 600 Ma. The time span between 630 and 600 Ma is a period of major tectono-metamorphic and magmatic activity in the Brasiliano belts of Brazil. This is due to the final closure of the Goiás Ocean and collision of the Amazon and São Francisco cratons (Pimentel *et al.* 1999). At the same time, the Paraná Block was welded to the São Francisco craton (Pimentel *et al.* 1999).

The coastal belts in southern Brazil have commonly been interpreted as equivalents to Pan-African belts in southwest Africa. However, in contrast to waning deformation in the Brasiliano belts in southern Brazil (Rio Grande do Sul and Santa Catarina) at about 600 Ma, the main orogenic deformations in the African counterparts are younger. Transpression in the Kaoko belt took place between 580 and 550 Ma (Coscombe, Hand & Gray, 2003); deformation of the Damara belt resulting from collision of the Kalahari and Congo cratons occurred at about 550 Ma (Prave, 1996). The belts in southwest Africa formed partly contemporaneously with deformation in the Araçuaí belt and some branches of the Ribeira belt, which starts in the 590–550 Ma time interval (Machado *et al.* 1996; Brueckner *et al.* 2000). Deformation in these areas therefore occurred about 50–70 Ma later than the main Brasiliano orogenic events in southern Brazil. Consequently, the Porongos and Dom Feliciano belts cannot be directly linked with Pan-African belts in southwest Africa like the Kaoko, Damara and Gariep belts, except for the observed long-lasting localized late- to post-orogenic strike-slip faulting in southern Brazil until 540 Ma which might be linked with the final stages of amalgamation of West Gondwana. Linkages of the South Brazilian and African belts are probably located on the present-day shelf regions off the coasts of eastern Brazil and western Africa.

Acknowledgements. Field work was partially supported by the Herrmann-Willkomm-Stiftung, Frankfurt a.M. Field support by the Centro de Estudos em Petrologia e Geoquímica (CPGq), Instituto de Geociéncias, Universidade Federal do Rio Grande do Sul, is highly appreciated. The visit and work in the geochronology lab at UFRGS, Porto Alègre, was made possible by financial support from the Deutscher Akademischer Austauschdienst (DAAD) and Coordenação de Aperfeiçoamento de Pessoal de Nível Superior (CAPES). We thank F. Bitencourt for supplying geological maps of the area. We appreciate constructive reviews by Mark Allen and an anonymous reviewer which helped to approve the manuscript.

References

ALMEIDA, F. F. M., BRITO NEVES, B. B. & CARNEIRO, C. D. R. 2000. The origin and evolution of the South American Platform. *Earth Science Reviews* **50**, 77–111.

BABINSKI, M., CHEMALE, F. JR, HARTMANN, L. A., VAN SCHMUS, W. R. & DA SILVA, L. C. 1996. Juvenile accretion at 750–700 Ma in southern Brazil. *Geology* **24**, 439–42

BABINSKI, M., CHEMALE, F. JR, VAN DER SCHMUS, W. R., HARTMANN, L. A. & DA SILVA, L. C. 1997. U–Pb and Sm–Nd Geochronology of the Neoproterozoic Granitic–Gneissic Dom Feliciano Belt, southern Brazil. *Journal of South American Earth Sciences* **3–4**, 263–74.

BASEI, M. A. S., SIGA, O. JR, MASQUELIN, H., HARARA, O. M., REIS NETO, J. M. & PRECOZZI, F. 2000. The Dom Feliciano Belt of Brazil and Uruguay and its Foreland Domain, the Rio de la Plata Craton. Framework, Tectonic Evolution and Correlation with Similar Provinces of Southwestern Africa. In *Tectonic Evolution of South America* (eds U. G. Cordani, E. J. Milani, A. Tomaz and D. A. Campos), pp. 311–34. 31st International Geological Congress, Sociedade Brasileira de Geologia Rio de Janeiro.

BOSSI, J. & GAUCHER, C. 2004. The Cuchilla Dionisio Terrane, Uruguay: An allochthonous block accreted in the Cambrian to SW-Gondwana. *Gondwana Research* **7**, 661–74.

BRUECKNER, H. K., CUNNINGHAM, D., ALKMIN, F. F. & MARSHAK, S. 2000. Tectonic implications of Precambrian Sm–Nd dates from the southern São Francisco craton and adjacent Araçuaí and Ribeira belts, Brazil. *Precambrian Research* **99**, 255–69.

CHEMALE, F. JR. 2000. Evolução Geológica do Escudo Sul-rio-grandense. In *Geologia do Rio Grande do Sul* (eds M. Holz and L. F. De Ros), pp. 13–52. Porto Alegre: CIGO/Universidade Federal do Rio Grande do Sul, Brazil.

CHEMALE, F. JR, HARTMANN, L. A. & DA SILVA, L. C. 1995. Stratigraphy and tectonism of the Brasiliano Cycle in southern Brazil. *Communications of the Geological Survey of Namibia* **10**, 151–66.

COSCOMBE, B., HAND, M. & GRAY, D. 2003. Structure of the Kaoko Belt, Namibia: progressive evolution of a classic transpressional orogen. *Journal of Structural Geology* **25**, 1049–81.

DEPAOLO, D. J. 1981. A neodymium and strontium isotopic study of the Mesozoic calc-alkaline granitic batholiths of the Sierra Nevada and Peninsular Ranges, California. *Journal of Geophysical Research* **68**, 10470–88.

FERNANDES, L. A. D. & KOESTER, E. 1999. The Neoproterozoic Dorsal de Canguçu strike-slip shear zone: its nature and role in the tectonic evolution of southern Brazil. *Journal of African Earth Sciences* **29**, 3–24.

FERNANDES, L. A. D., MENEGAT, R., COSTA, A. F. U., KOESTER, E., PORCHER, C. C., TOMMASI, A., KRAEMER, G., RAMGRAB, G. & CAMOZZO, E. 1995. Evolução tectõnica do Cinturão Dom Feliciano no Escudo Sul-riograndense: Parte I – Uma contribução a partir do registro geológico. *Revista Brasileira de Geociéncias* **25**, 351–74.

Fernandes, L. A. D., Tommasi, A. & Porcher, C. C. 1992. Deformation patterns in the southern Brazilian branch of the Dom Feliciano Belt: A reappraisal. *Journal of South American Earth Sciences* **5**, 77–96.

Frantz, J. C. & Botelho, N. F. 2000. Neoproterozoic Granitic Magmatism and Evolution of the Eastern Dom Feliciano Belt in southernmost Brazil: A Tectonic Model. *Gondwana Research* **3**, 7–19.

Frantz, J. C., Botelho, N. F., Pimentel, M. M., Potrel, A., Koester, E. & Teixeira, R. S. 1999. Relações isotópicas Rb–Sr e Sm–Nd e idades do magmatismo granítico Brasiliano da região leste do Cinturão Dom Feliciano no Rio Grande do Sul: Evidéncias de retrabalhamento de crosta continetal Palaeoproterozóica. *Revista Brasileira de Geociéncias* **29**, 227–32.

Frantz, J. C. & Nardi, L. V. S. 1992. O Magmatismo Granítico da região Oriental do Escudo Sul-rio-grandense. Uma Revisão. *Pesquisas* **19**, 183–9.

Frantz, J. C., Remus, M. V. D. & Hartmann, L. A. 2000. Geological units, ages and tectonic evolution of the Neoproterozoic Dom Feliciano Belt, southernmost Brazil – a review. *Revista Brasileira de Geociéncias* **30**, 55–7.

Gaucher, C., Chiglino, L. & Peçoits, E. 2003. Southernmost exposures of the Arroyo del Soldado Group (Vendian to Cambrian, Uruguay): Palaeogeographic implications for the amalgamation of W-Gondwana. *Gondwana Research* **7**, 701–14.

Gromet, L. P., Dymek, R. F., Haskin, L. A. & Korotev, R. L. 1984. The "North American Shale Composite": its compilation, major and trace element characteristics. *Geochimica et Cosmochimica Acta* **48**, 2469–82.

Hartmann, L. A. 1998. Deepest Exposed Crust of Brazil – Geochemistry of Paleoproterozoic Depleted Santa Maria Chico Granulites. *Gondwana Research* **1**, 331–41.

Hartmann, L. A., Campal, N., Santos, J. O. S., McNaughton, N. J., Bossi, J., Schipilov, A. & Lafon, J.-M. 2001. Archean crust in the Rio de la Plata Craton, Uruguay – SHRIMP U–Pb zircon reconnaissance geochronology. *Journal of South American Earth Sciences* **14**, 557–70.

Hartmann, L. A., Leite, J. A. D., Da Silva, L. C., Remus, M. V. D., McNaughton, N. J., Groves, D. I., Fletcher, I. R., Santos, J. O. S. & Vasconcellos, M. A. Z. 2000. Advances in SHRIMP geochronology and their impact on understanding the tectonic and metallogenic evolution of southern Brazil. *Australian Journal of Earth Sciences* **47**, 829–44.

Hartmann, L. A., Nardi, L. V. S., Formoso, L. L., Remus, M. V. D., De Lima, E. F. & Mexias, A. S. 1999. Magmatism and Metallogeny in the Crustal Evolution of Rio Grande do Sul Shield, Brazil. *Pesquisas* **26**, 45–63.

Hartmann, L. A., Philipp, R. P., Liu, D., Wang, L., Santos, J. O. S. & Vasconcellos, M. A. Z. 2004. Paleoproterozoic Magmatic Provenance of Detrital Zircons, Porongos Complex Quartzites, Southern Brazilian Shield. *International Geology Review* **46**, 127–57.

Hartmann, L. A., Porcher, C. C. & Remus, M. V. D. 2000. Evolução das rochas metamórficas do Rio Grande do Sul. In *Geologia do Rio Grande do Sul* (eds M. Holz, and L. F. De Ros), pp. 79–118. Porto Alegre: CIGO/Universidade Federal do Rio Grande do Sul, Brazil.

Hartmann, L. A. & Santos, J. O. 2004. Predominance of high Th/U, magmatic zircon in Brazilian Shield sandstones. *Geology* **32**, 73–6.

Hartmann, L. A., Santos, J. O. S., Leite, J. A. D., Porcher, C. C. & McNaughton, N. J. 2003. Metamorphic evolution and U–Pb zircon SHRIMP geochronology of the Belizário ultramafic amphibolite, Encantadas Complex, southernmost Brazil. *Anais da Academia Brasileira de Ciéncias* **75**, 393–403.

Jost, H. 1982. Condições do metamorfismo regional de uma parte da faixa de dobramentos de Tijucas no Rio Grande do Sul-RS. *Acta Geologica Leopoldensia* **12**, 3–32.

Jost, H. & Bitencourt, M. F. 1980. Estratigrafia e tectônica de uma fração da Faixa de Dobramentos de Tijucas no Rio Grande do Sul. *Acta Geologica Leopoldensia* **4**, 27–60.

Jost, H. & Hartmann, L. A. 1984. Provincia Mantiqueira – Sector Meridional. In *O Pre-Cambriano do Brasil* (eds F. F. M. Almeida and Y. Hasui), pp. 345–68. São Paulo: Edgard Blucher Ltda.

Koester, E., Soliani, E. Jr, Fernandes, L. A. D., Kraemer, G. & Tommasi, A. 1997. Geocronologia Rb–Sr e K–Ar dos granitóides sintectônicos à Zona de Cisalhamento Transcorrente Dorsal de Canguçu na região de Encruzilhada do Sul, RS. *Pesquisas* **24**, 67–77.

Koppe, J. C. & Hartmann, L. A. 1988. Geochemistry of the Bossoroca greenstone Belt, southernmost Brazil. *Geochimica Brasiliensis* **2**, 167–74.

Leite, J. A. D., Hartmann, L. A., Fernandes, L. A. D., McNaughton, N. J., Soliani, E. Ã. Jr, Koester, E., Santos, J. O. S. & Vasconcellos, M. A. Z. 2000. Zircon U–Pb SHRIMP dating of gneissic basement of the Dom Feliciano Belt, southernmost Brazil. *Journal of South American Earth Sciences* **13**, 739–50.

Leite, J. A. D., Hartmann, L. A., McNaughton, N. J. & Chemale, F. Jr. 1998. SHRIMP U/Pb Zircon Geochronology of Neoproterozoic Juvenile and Crustal-Reworked Terranes in Southernmost Brazil. *International Geology Review* **40**, 688–705.

Machado, N., Valladares, C., Heilbron, M. & Valeriano, C. 1996. U–Pb geochronology of the central Ribeira belt (Brazil) and implications for the evolution of the Brazilian Orogeny. *Precambrian Research* **79**, 347–61.

Mantovani, M. S. M., Hawkesworth, C. J. & Basei, M. A. S. 1987. Nd and Pb isotope studies bearing on crustal evolution of Southeastern Brazil. *Revista Brasileira de Geociéncias* **17**, 263–8.

Nabholz, W. K. & Voll, G. 1963. Bau und Bewegung im Gotthard-massivischen Mesozoikum bei Ilnaz (Graubünden). *Eclogae Geologicae Helvetiae* **56**, 755–808.

Paim, P. S. G., Chemale, F. Jr & Lopes, R. C. 2000. A Bacia do Camaquã. In *Geologia do Rio Grande do Sul* (eds M. Holz, and L. F. De Ros), pp. 251–74. Porto Alegre: CIGO/Universidade Federal do Rio Grande do Sul, Brazil.

Philipp, R. P., Mesquita, M. J., Gomes, M. E. B. & Almeida, D. P. M. 1993. Reconhecimento estrutural e geoquímico dos Granitóides Brasilianos da região de Pelotas, RS. *Pesquisas* **20**, 3–13.

Philipp, R. P., Nardi, L. V. S. & Bitencourt, M. F. 2000. O Batólito Pelotas no Rio Grande do Sul. In *Geologia do Rio Grande do Sul* (eds M. Holz, and L. F. De Ros), pp. 133–60. Porto Alegre: CIGO/Universidade Federal do Rio Grande do Sul, Brazil.

PORCHER, C. C. & FERNANDES, L. A. D. 1990. Relações embasamento-cobertura na porção occidental do Cinturão Dom Feliciano: um esboço estrutural. *Pesquisas* **17**, 72–84.

PRAVE, A. R. 1996. Tale of three cratons: Tectonostratigraphic anatomy of the Damara orogen in northwestern Namibia and the assembly of Gondwana. *Geology* **24**, 1115–18.

REMUS, M. V. D, HARTMANN. L. A., MCNAUGHTON, N. J., GROVES, D. I. & FLETCHER, I. R. 2000*a*. The link between hydrothermal epigenetic copper mineralization and the Caçapava Granite of the Brasiliano Cycle in southern Brazil. *Journal of South American Earth Sciences* **13**, 191–216.

REMUS, M. V. D., HARTMANN, L. A., MCNAUGHTON, N. J., GROVES, D. I. & REISCHL, J. L. 2000*b*. Distal Magmatic-Hydrothermal Origin for the Camaquã Cu (Au–Ag) and Santa Maria Pb, Zn (Cu–Ag) deposits, Southern Brazil. *Gondwana Research* **3**, 155–74.

REMUS, M. V. D., HARTMANN, L. A. & RIBEIRO, M. 1991. Nota sobre a geologia dos metamorfitos de pressão intermediária e granitóides associados da região de Pinheiro Machado/RS. *Acta Geologica Leopoldensia* **34**, 175–90.

REMUS, M. V. D., PHILIPP, R. P., FACCINI, U. F. & JUNGES, S. L. 1990. Contribução ao estudo geológico-estrutural dos Gnaisses Encantadas e as relações com as supracrustais Porongos na região de Santana da Boa Vista/RS. In *Congresso Brasileiro de Geologia 36, Natal* (ed. Sociedade Brasileira de Geologia Rio de Janeiro), pp. 2356–70. *Anais de Congresso Brasileiro de Geologia 36, SBG* **5**. Sociedade Brasileira de Geologia Rio de Janeiro.

REMUS, M. V. D., TEDESCO, M. A., PHILIPP, R. P. & FACCINI, U. F. 1987. Evolução estrutural da unidade Porongos a sul do Rio Camaquã, RS. In *Simpósio Sul-Brasileiro de Geologia 3, Curitiba* (ed. Sociedade Brasileira de Geologia Rio de Janeiro), pp. 223–44. *Anais Simpósio Sul-Brasileiro de Geologia 3, SBG* **1**. Sociedade Brasileira de Geologia Rio de Janeiro.

SAALMANN, K. 2004. Deformation of the Neoproterozoic juvenile Cambaí magmatic arc complex and syntectonic granites during the Brasiliano orogenic cycle in southernmost Brazil. *Zeitschrift der Deutschen Geologischen Gesellschaft* **154**(4), 557–77.

SAALMANN, K., HARTMANN, L. A., REMUS, M. V. D., KOESTER, E. & CONCEIÇÃO, R. V. 2005. Sm–Nd isotope geochemistry of metamorphic volcano-sedimentary successions in the São Gabriel Block, southernmost Brazil: evidence for the existence of juvenile Neoproterozoic oceanic crust to the east of the Rio de la Plata craton. *Precambrian Research* **136**, 159–75.

SAALMANN, K., REMUS, M. V. D. & HARTMANN, L. A. 2005. Geochemistry and crustal evolution of volcano-sedimentary successions and orthogneisses in the Sao Gabriel Block, southernmost Brazil – relics of Neoproterozoic magmatic arcs. *Gondwana Research* **8**, 143–61.

SAALMANN, K., REMUS, M. V. D & HARTMANN, L. A. In press. Tectonic evolution of the Neoproterozoic juvenile São Gabriel Block, southern Brazil – constraints on Brasiliano orogenic evolution of the Rio de la Plata cratonic margin. *Journal of South American Earth Sciences.*

SÁNCHEZ BETTUCCI, L., COSARINSKY, M. & RAMOS, V. A. 2001. Tectonic setting of the Late Proterozoic Lavalleja Group (Dom Feliciano belt), Uruguay. *Gondwana Research* **4**, 395–407.

SANTOS, J. O. S., HARTMANN, L. A., BOSSI, J., CAMPAL, N., SCHIPILOV, A., PIÑEYRO, D. & MCNAUGHTON, N. J. 2003. Duration of the Trans-Amazonian Cycle and its correlation within South America based on U–Pb SHRIMP geochronology of La Plata Craton, Uruguay: *International Geology Review* **45**, 27–48.

SETH, B., KRÖNER, A., MEZGER, K. NEMCHIN, A. A., PIDGEON, R. T. & OKRUSCH, M. 1998. Archaean to Neoproterozoic magmatic events in the Kaoko belt of NW Namibia and their geodynamic significance. *Precambrian Research* **92**, 341–63.

SILVA, C., HARTMANN, L. A., MCNAUGHTON, N. J. & FLETCHER, I. R. 1999. SHRIMP U/Pb zircon timing of Neoproterozoic granitic magmatism and deformation in the Pelotas Batholith in southernmost Brazil. *International Geology Review* **41**, 531–51.

SILVA, C., HARTMANN, L. A., MCNAUGHTON, N. J. & FLETCHER, I. R. 2000. Zircon U/Pb SHRIMP dating of a Neoproterozoic overprint in Paleoproterozoic granitic–gneissic terranes, southern Brazil. *American Mineralogist* **85**, 649–68.

STIPP, M., STÜNITZ, H., HEILBRONNER, R. & SCHMID, S. M. 2002. The eastern Tonale Fault zone: A 'natural laboratory' for crystal plastic deformation of quartz over a temperature range from 250 to 700°C. *Journal of Structural Geology* **24**, 1861–84.

SUN, S.-S. & MCDONOUGH, W. F. 1989. Chemical and isotopic systematics of oceanic basalts: implications for mantle composition and processes. In *Magmatism in the Ocean Basins* (eds A. D. Saunders and M. J. Norry), pp. 313–45. Geological Society of London, Special Publication no. 42.

TAYLOR, R. S. & MCLENNAN, S. M. 1985. *The continental crust: its composition and evolution.* Oxford: Blackwell.

TOMMASI, A., VAUCHEZ, A., FERNANDES, L. A. D. & PORCHER, C. C. 1994. Magma-assisted strain localization in an orogen-parallel transcurrent shear zone of southern Brazil. *Tectonics* **13**, 421–37.

TROMPETTE, R. 1994. Geology of Western Gondwana (2000–500 Ma). Pan-African-Brasiliano aggregation of South America and Africa. Rotterdam: Balkema, 350 pp.

TULLIS, J. & YUND, R. A. 1987. Transition from cataclastic flow to dislocation creep of feldspar: Mechanisms and microstructures. *Geology* **15**, 606–9.

UNRUG, R. 1997. Rodinia to Gondwana: The geodynamic Map of Gondwana Supercontinent Assembly. *Geological Society of America (GSA) Today* **7**, 1–6.

VOLL, G. 1960. New work of petrofabrics. *Liverpool Manchester Geological Journal* **2**, 503–67.